Spatiotemporally Graded NMDA Spike/Plateau Potentials in Basal Dendrites of Neocortical Pyramidal Neurons

Article *in* Journal of Neurophysiology · June 2008

DOI: 10.1152/jn.00011.2008 · Source: PubMed

J Neurophysiol 99: 2584–2601, 2008.
First published March 12, 2008; doi:10.1152/jn.00011.2008.

Spatiotemporally Graded NMDA Spike/Plateau Potentials in Basal Dendrites of Neocortical Pyramidal Neurons

Guy Major,[1] Alon Polsky,[2] Winfried Denk,[3] Jackie Schiller,[2] and David W. Tank[1]
[1]*Molecular Biology and Physics, Princeton University, Princeton, New Jersey;* [2]*Physiology, Technion Medical School, Haifa, Israel; and* [3]*Max-Planck Institut für Medizinische Forschung, Heidelberg, Germany*

Submitted 4 January 2008; accepted in final form 5 March 2008

Major G, Polsky A, Denk W, Schiller J, Tank DW. Spatiotemporally graded NMDA spike/plateau potentials in basal dendrites of neocortical pyramidal neurons. *J Neurophysiol* 99: 2584–2601, 2008. First published March 12, 2008; doi:10.1152/jn.00011.2008. Glutamatergic inputs clustered over ~20–40 μm can elicit local *N*-methyl-D-aspartate (NMDA) spike/plateau potentials in terminal dendrites of cortical pyramidal neurons, inspiring the notion that a single terminal dendrite can function as a decision-making computational subunit. A typical terminal basal dendrite is ~100–200 μm long: could it function as *multiple* decision-making subunits? We test this by sequential focal stimulation of multiple sites along terminal basal dendrites of layer 5 pyramidal neurons in rat somatosensory cortical brain slices, using iontophoresis or uncaging of brief glutamate pulses. There was an approximately sevenfold spatial gradient in average spike/plateau amplitude measured at the soma, from ~3 mV for distal inputs to ~23 mV for proximal inputs. Spike/plateaus were NMDA receptor (NMDAR) conductance-dominated at all locations. Large Ca^{2+} transients accompanied spike/plateaus over a ~10- to 40-μm zone around the input site; smaller Ca^{2+} transients extended approximately uniformly to the dendritic tip. Spike/plateau duration grew with increasing glutamate and depolarization; high Ca^{2+} zone size grew with spike/plateau duration. The minimum high Ca^{2+} zone half-width (just above NMDA spike threshold) increased from distal (~10 μm) to proximal locations (~25 μm), as did the NMDA spike glutamate threshold. Depolarization reduced glutamate thresholds. Simulations exploring multi-site interactions based on this demonstrate that if appropriately timed and localized inputs occur in vivo, a single basal dendrite could correspond to a cascade of *multiple* co-operating dynamic decision-making subunits able to retain information for hundreds of milliseconds, with increasing influence on neural output from distal to proximal. Dendritic NMDA spike/plateaus are thus well-suited to support graded persistent firing.

INTRODUCTION

The majority of inputs to pyramidal neurons in cerebral cortex synapse onto "thin" dendrites with diameters <1 μm, such as terminal basal dendrites (Larkman 1991a,b). Their computational power is much debated. Do thin dendrites simply collect inputs and relay them to the cell body (Cash and Yuste 1999; Rall 1977)? Or can a single thin dendrite act as nonlinear, decision-making computational "subunit," i.e., a device receiving graded inputs that emits a clear signal above some defined threshold (Losonczy and Magee 2006; Poirazi et al. 2003; Wei et al. 2001)? Terminal basal dendrites are generally around 100–200 μm long (Larkman 1991a) with extensive cable properties (Nevian et al. 2007). Can a single thin dendrite contain a sliding subunit detecting clustered inputs (Nevian et al. 2007; Polsky et al. 2004), or can it be equivalent to a string or cascade of *multiple* interacting subunits or an even more complex device such as a neural temporal integrator (Loewenstein and Sompolinsky 2003)? These are important unresolved questions relevant to the fundamental computational principles underlying brain function.

A number of in vitro studies have probed input-output relations of thin dendrites, using a variety of stimulation techniques including sensory inputs (in the retina, Euler et al. 2002), glutamate uncaging and iontophoresis, and local synaptic stimulation. These have been combined with a variety of recording techniques such as calcium- or voltage-sensitive dye imaging or whole cell recording directly from thin dendrites (Nevian et al. 2007). Fast local sodium spikes or spikelets lasting up to a few milliseconds have been described in basal and apical oblique dendrites of hippocampal and cortical pyramidal neurons (Ariav et al. 2003; Losonczy and Magee 2006; Milojkovic et al. 2005b; Nevian et al. 2007). In addition, brief focal glutamatergic stimulation of thin dendrites of both neocortical and hippocampal pyramidal neurons can evoke slower spike/plateau potentials lasting 20 to hundreds of milliseconds (Ariav et al. 2003; Cai et al. 2004; Holthoff et al. 2004; Milojkovic et al. 2004, 2005a; Oakley et al. 2001a,b; Polsky et al. 2004; Schiller et al. 2000; Wei et al. 2001).

Depending on their morphology and mixes of active conductances, thin dendrites from different cell classes in different brain areas may well comprise different effective numbers of computational subunits, and this may depend on patterns of activity and overall brain state. In neocortical layer 5 and layer 2/3 pyramidal neuron basal dendrites, spike/plateaus have been reported to be predominantly *N*-methyl-D-aspartate receptor (NMDAR) mediated (Gordon et al. 2006; Schiller et al. 2000). They can be re-initiated at higher stimulus levels in sodium and calcium channel blockers but are completely abolished by the NMDAR blockers 2-amino-5-phosphonovaleric acid (APV) (Schiller et al. 2000), CPP or MK801 (Polsky et al. 2004; G. Major and D. W. Tank, unpublished). Models suggest a minor "helper" role for sodium and calcium channels and a dominant role for NMDAR channels, carrying ~80% of the overall charge (Schiller et al. 2000), hence the term "NMDA spike." Calcium imaging data and modeling suggest that NMDA spikes evoked by focal stimulation are mediated in large part by a zone of activated NMDAR conductance localized to within a few tens of micrometers of the input site (Schiller et al. 2000). Two synaptic inputs onto a single basal dendrite

Address for reprint requests and other correspondence: G. Major, School of Biosciences, Cardiff University, Museum Ave., Cardiff, CF10 3US, Wales, UK (E-mail: majorg@cardiff.ac.uk).

The costs of publication of this article were defrayed in part by the payment of page charges. The article must therefore be hereby marked "*advertisement*" in accordance with 18 U.S.C. Section 1734 solely to indicate this fact.

can interact progressively more supralinearly as the inputs are moved closer together (Polsky et al. 2004). Once the stimulating electrodes are within ~40 μm of one another, summation can be strongly supralinear with recruitment of an NMDA spike if the stimuli are of appropriate strength (individually subthreshold, together suprathreshold). This led to the suggestion that each dendrite can function as a single computational subunit with a sliding integration window a few tens of micrometers long, which can perform a sigmoidal input-output transform on spatiotemporally clustered inputs. In that study, however, the distal stimulation site was held fixed while the proximal stimulation site was moved toward it, so a full exploration of the number of potential subunits along the entire dendrite was not performed. There have been preliminary indications that there may be differences between local dendritic spike/plateaus in different parts of a given basal dendrite. It is harder to evoke proximal than distal NMDA spikes using synaptic stimulation, and different plasticity rules seem to apply to proximal and distal compartments of basal dendrites (Gordon et al. 2006). In addition, computer simulations and experiments partially exploring different subregions of basal dendrites suggest that proximal basal dendritic spike/plateaus have larger somatic amplitudes than distal spike/plateaus (Milojkovic et al. 2004; Rhodes 2006; Schiller et al. 2000; G. Major, unpublished data). However, a full characterization of this trend along the entire length of particular single basal dendrites has not been reported.

Similar local plateau potentials have been found in hippocampal CA1 pyramidal neuron apical tuft/oblique dendrites (Cai et al. 2004; Wei et al. 2001). Cd^{2+} block of these plateaus and calcium imaging with easily saturable high-affinity indicators were interpreted as showing that a suprathreshold stimulus leads to an all-or-none calcium plateau potential throughout the input dendrite (bistability). This would mean that each apical tuft or oblique dendrite can function as a *single* computational subunit. However, no explicit tests of plateau reinitiation at higher stimulus levels in Cd^{2+} were reported, and NMDAR antagonists blocked the plateaus, which may therefore actually have been NMDAR dominated. Consistent with this, close inspection of the calcium imaging data from that study suggests there may in fact have been a high calcium zone around the input site that could perhaps be revealed more clearly by using lower-affinity calcium indicators (Cai et al. 2004; their Figs. 4 and 7 and supplementary movies). Furthermore, different inputs sites along a given dendrite were not stimulated to check for location dependence of the somatic amplitudes of the plateau potentials. These uncertainties leave open the possibility that single CA1 tuft or oblique dendrites may sometimes be equivalent to *multiple* computational subunits.

Patterned 2-photon glutamate uncaging has been used to probe the input-output relations of single apical oblique dendrites of CA1 pyramidal cells (Losonczy and Magee 2006). Sufficiently strong glutamate pulses concentrated in a 6-ms window trigger a fast local sodium spike or spikelet with a slower NMDAR-dependent component. These data were interpreted as showing that each oblique dendrite can function as a *single* computational subunit, both for spatially clustered and distributed near-synchronous inputs. However, proximal clustered inputs can produce dendritic spikes with somatic amplitudes that are nearly twice those of distal clustered inputs on the same branch (Losonczy and Magee 2006). In addition, the entire length of single branches was not explored fully with clustered inputs. Again the possibility remains, therefore, that single oblique dendrites in these cells may be capable of functioning as more than one subunit—provided of course that input patterns in vivo can be sufficiently clustered.

In the light of the above, the main aim of the current study is to ask the question, can a single terminal basal dendrite of a neocortical layer 5 pyramidal neuron correspond to a string of *multiple* interacting decision-making computational subunits? To this end, we systematically explore how spike/plateau potentials evoked by brief focal glutamate pulses vary with input location along the length of single basal dendrites, and we generate detailed spatial maps of the associated calcium transients. We investigate which regions of a given dendrite can support a local spike/plateau, what fraction of the dendrite is required at each location, and what proximal-to-distal differences there are in somatic amplitude and the underlying dendritic ionic conductances. To assess whether putative subunits along a single dendrite can potentially *interact*, we also explore the voltage dependence of the glutamate thresholds of the spike/plateaus. In other words, could the generation of a spike/plateau at one location be influenced, in principle, by depolarization propagating along the dendritic cable from spike/plateaus elsewhere? The results of these experiments suggest that basal dendrites could have very versatile computational capabilities based on spatiotemporally graded NMDA spike/plateaus. We perform simulations exploring multi-site interactions, which demonstrate that if appropriately timed and spatially localized patterns of input occur in vivo, then a single terminal basal dendrite could indeed correspond to a cascade of multiple cooperating NMDAR-dominated dynamic computational subunits, although this remains to be demonstrated directly in experiments.

METHODS

Electrophysiology

Sprague-Dawley rats aged 23–41 days were anesthetized with isoflurane and decapitated, and the brain was removed under cold artificial cerebrospinal fluid [ACSF, composed of (in mM) 125 NaCl, 26 $NaHCO_3$, 3.6 KCl, 1 $MgCl_2$, 2 $CaCl_2$, 10 glucose, bubbled with 95% O_2-5% CO_2]. Coronal somatosensory cortical slices 300 μm thick were cut, incubated submerged for 30 min at 35°C, then transferred to a 20–22°C interface holding chamber. Individual slices were placed in the recording chamber and held at 35–37°C with ACSF flowing over both surfaces. Patch pipettes were pulled from borosilicate glass (1.2 mm OD, 0.6 mm ID, filament, FHC, Bowdoinham, ME), resistance: 3.5–8 MΩ, tip diameters: 2–3 μm, filled with (in mM) 140 KGluconate, 10 HEPES, 2 $MgCl_2$, 3 ATP-Na_2, 0.3 GTP-Na, and 0.1 Magnesium Green, pH 7.3, osmolarity 275 mosM. Somatic whole cell recordings were made from large layer 5 pyramidal neurons. Cells were loaded with indicator for ~20 min (Fig. 1). Soma membrane potential was recorded with a Dagan BVC700 amplifier, amplified, filtered at 5 kHz (8-pole Bessel, FLA-01, Cygnus Technology), and digitized at 10 kHz (Axon Digidata 1322A, Clampex software, Molecular Devices). To reduce spread in the data, cells with peak input resistances at −72 mV of >35 MΩ were excluded from the amplitude-distance analysis, although they yielded qualitatively similar results (generally with bigger spike/plateau amplitudes).

Imaging

Calcium transients in basal dendrites were imaged using a custom-built two-photon microscope ("Moveable Objective Microscope," Denk W., Sutter Instruments, Novato, CA) with a diode laser pumping a Ti:Sapphire femtosecond pulse laser (Verdi V10 and Mira 900F, Coherent, Santa Clara, CA) tuned to 860–920 nm, infrared filter, photomultiplier (Hamamatsu E850-13), ×40 long working distance NA 0.8 IR objective and ScanImage software (Pologruto et al. 2003). In earlier experiments, we found that when cells were filled with the high-affinity calcium indicator Calcium Green-1, which has a K_d of ~190 nM (Haugland and Free 2005a), subthreshold responses were associated with fluorescence transients, but suprathreshold spike/plateau fluorescence waveforms reached elevated levels that remained constant for long periods, indicative of severe indicator saturation (not shown). This saturation led to misleading calcium maps with the difference between the high-input site and distal lower Ca^{2+} zones obscured (see following text). Despite its name, Magnesium Green has proved to be a useful calcium indicator (Koester and Sakmann 2000) that we chose to use because of its relatively high resting fluorescence, large maximal fluorescence change, and low Ca^{2+} affinity (K_d ~6 μM) (Haugland and Free 2005b; Zhao et al. 1996). Compared with other higher-affinity indicators, the low Ca^{2+} affinity of Magnesium Green reduces Ca^{2+} buffering and slowing and saturation of fluorescence transients associated with changes in Ca^{2+}. The high resting fluorescence facilitates aiming and gives a good signal-to-noise for $\Delta F/F$ relative fluorescence measurements. Many other commonly used calcium indicators also bind other divalent cations such as Mg^{2+} with changes in fluorescence (Haugland and Free 2006). Magnesium Green has very low Mg^{2+} affinity, K_d ~1 mM (Haugland and Free 2005b). With our filling solution, intracellular Mg^{2+} ions are mostly complexed to much higher affinity Mg^{2+} buffers such as ATP, K_d ~40 μM (Nakayama et al. 1994).

Glutamate iontophoresis

Sharp double-barreled electrodes were filled with 160 mM Na glutamate, pH 8.6 in 1 barrel, resistance, 300–400 MΩ) and 1 mM fluorescein in the other. The electrode was advanced under visual control (2-photon microscope) to within 1–2 μm of a basal dendrite (Fig. 1*A*, Supplementary Fig. S1*A*[1]); 5-ms negative pulses, absolute amplitude typically ≤300 nA, were injected into the glutamate barrel using a modified Axoclamp-2B amplifier (Molecular Devices; see Supplementary METHODS), with the absolute amplitude of the backing current <1 nA. To reduce phototoxicity, 512-ms square frame scans were used for most glutamate and voltage threshold tests and amplitude-distance explorations (Supplementary Fig. S1, *A* and *B*) with the input site in focus in the center of the field, and the glutamate pulse timed so that the peak of the local fluorescent transient was "caught" by the scan (Supplementary Fig. S1*E*). This was verified by use of faster rectangle scans (64 ms/frame) and line scans (2 ms/line). Rectangle and line scans were used for more detailed calcium profiling along dendrites.

Data analysis

Custom software was written in Matlab (the Mathworks, Natick, MA). Bridge balance was fine-tuned off-line. The curvilinear distance of input sites from the edge of the cell body was computed as the sum of the Pythagorean lengths of contiguous short linear segments on the image stacks. Fluorescence transients were analyzed using standard techniques, subtracting background, and normalizing by baseline fluorescence F, and, in the case of detailed calcium profiles, calculating medians from data at multiple microscope positions and focal depths, rejecting noisy data from out-of-focus faint segments of dendrite (which could also generate artifactually high $\Delta F/F$ ratios). The iontophoretic electrode and regions outside the dendrite were masked out with a semi-automated algorithm. Rectangular regions of interest (ROIs) were defined taking account of signal-to-noise and spatial variations in the calcium transients. Unless stated otherwise, results are quoted as means ± SD and 2-tailed *t*-tests were performed.

Glutamate uncaging

Slices from 25- to 33-day-old rats were used. MNI-glutamate (Tocris, Bristol, UK), (Matsuzaki et al. 2001) was delivered locally to a dendrite using pressure ejection (5–10 mbar) from an electrode (2 μm diam, containing 5–10 mM caged glutamate, 20–50 μm from dendrite) and was photolysed by ~1-ms pulses of a 361 nm UV-laser beam (Enterprise 2, Coherent, Palo Alto, CA) using point scan mode. Solutions were as in Polsky et al. (2004). Cells were imaged with a 60X, 0.9 NA water objective and a Fluoview 500 confocal system on an upright BX51WI microscope (Olympus, Tokyo, Japan).

Modeling

Simulations were performed using NEURON (Carnevale and Hines 2006), time step: 25 μs, temperature: 35 °C. A detailed branching compartmental model was based on a reconstructed layer 5 pyramidal cell (Larkman et al. 1992) with dendritic spine area incorporated into dendritic shafts (Stratford et al. 1989). The model cell had 50 basal and 49 apical dendritic branches, resting potential: −75 mV, R_m: 10,000 Ωcm^2, C_m: 0.8 μFcm^{-2}, giving a passive membrane time constant of 8 ms within the experimentally observed range (Mason and Larkman 1990). An R_i of 100 Ωcm in more proximal dendrites with diameters >1.2 μm after spine collapse procedure and 120 Ωcm in more distal dendrites was found to give the same spread of spike/plateau amplitudes as observed experimentally. Higher R_i's led to proximal plateaus that were too small at the soma, lower R_i's led to distal plateaus that were too big. It was not possible in the purely passive model to match the spatial gradient with a uniform R_i. For simplicity, unless otherwise stated, no voltage-dependent conductances other than NMDAR conductances were included, a reasonable first approximation in the light of the relatively minor contributions of sodium and calcium channels to local basal dendritic spike/plateaus at all locations tested. The input dendrite was divided into 24 electrical compartments. Iontophoretic or uncaging pulses of glutamate (1–5 ms long) were approximated as impulses (instantaneous pulses) as were glutamate transients from single synaptic inputs (from single presynaptic action potentials). Alpha-amino-3-hydroxy-5-methyl-4-isoxazole propionic acid (AMPA) receptor excitatory inputs were modeled as double exponentials with τ_{on} of 0.2 and τ_{off} of 2 ms, reversal potential 0 mV, and a peak AMPAR conductance of 0.875 nS at each input site. Unless otherwise specified, NMDAR conductances were based on previous studies (Ascher and Nowak 1988; Brodin et al. 1991; D'Angelo et al. 1994; Schiller et al. 2000). Each NMDA conductance response to a glutamate impulse had a triple-exponential "envelope" time course and a sigmoidal voltage dependence given by

$$g_{NMDA} = g_{maxNMDA}[-e^{-t/\tau_{on}} + f_{fast}e^{-t/\tau_{off1}} + (1 - f_{fast})e^{-t/\tau_{off2}}]p,$$

$$f_{fast} = f_0 + f_{slope}V, f_0 = 0.515, f_{slope} = -0.003125\ mV^{-1}$$

with voltage-dependent time constants given by

$$\tau_{on} = \tau_{on0} + \tau_{onslope}V,$$

$\tau_{off1} = \tau_{off1\_0} + \tau_{off1slope}V$, $\tau_{off2} = \tau_{off2\_0} + \tau_{off2slope}V$, τ_{on0} = 2.915 ms, $\tau_{onslope}$ = −0.004125 ms/mV, τ_{off1_0} = 61.5 ms, $\tau_{off1slope}$ = 0.5625 ms/mV, τ_{off2_0} = 352.5 ms, $\tau_{off2slope}$ = 5.7375 ms/mV, all at

[1] Experiments carried out at 1 and 3. Pilot experiments carried out at Bell Laboratories, Lucent Technologies, Murray Hill, NJ (Major, Denk, Tank).

The online version of this article contains supplemental data.

28.5°C (D'Angelo et al. 1994), which were then adjusted to 35°C using a q_{10} temperature dependence of 3 (i.e., time constants were divided by $3^{(35-28.5)/10} = 2.042$).

The voltage dependence p of the Magnesium unblocking had forward and backward rate constants

$$\alpha = A_\alpha e^{V/V_{spread\alpha}}, \qquad A_\alpha = 5.4\ ms^{-1},\ V_{spread\alpha} = 47\ mV,$$

and

$$\beta = A_\beta[Mg^{2+}]e^{V/V_{spread\beta}},\ A_\beta = 0.61\ mM^{-1}ms^{-1},\ V_{spread\beta} = 17\ mV$$

(Ascher and Nowak 1988), assumed $[Mg^{2+}] = 1.8$ mM (Brodin et al. 1991), all at 20°C and adjusted to 35°C using a q_{10} temperature dependence of 3, i.e., rates were multiplied by 5.196. These parameters give a sigmoidal steady-state voltage dependence

$$[1 + e^{-(V-V_{1/2})/V_{spread}}]^{-1},$$

with a half-activation voltage $V_{1/2}$ of −19.9 mV and a V_{spread} of 12.48 mV. In this scheme, $g_{maxNMDA}$ is 14% above actual peak openable NMDA conductance. During simulations for Supplementary Fig. S3, peak envelope (openable) NMDA conductance ranged from 173 to 28 nS (proximal to tip), and peak opened NMDAR conductance ranged from 126 to 21 nS (proximal to tip). Inclusion of low densities of sodium and calcium channels as in Schiller et al. (2000) reduced the amount of NMDA conductance required for a spike/plateau and reproduced the rise in threshold seen with sodium and/or calcium channel blockade (not shown). NEURON files available on request.

RESULTS

Local dendritic spike/plateaus can be evoked by brief focal pulses of glutamate onto a single basal dendrite

Terminal basal dendrites of large layer 5 neocortical pyramidal neurons were stimulated focally by iontophoresing 5-ms pulses of glutamate from a nearby sharp electrode (using negative current). The electrode tip was within 1 or 2 μm of the dendrite (Figs. 1*A* and Supplementary S1). Somatic voltage was recorded while imaging the dendrite with a two-photon

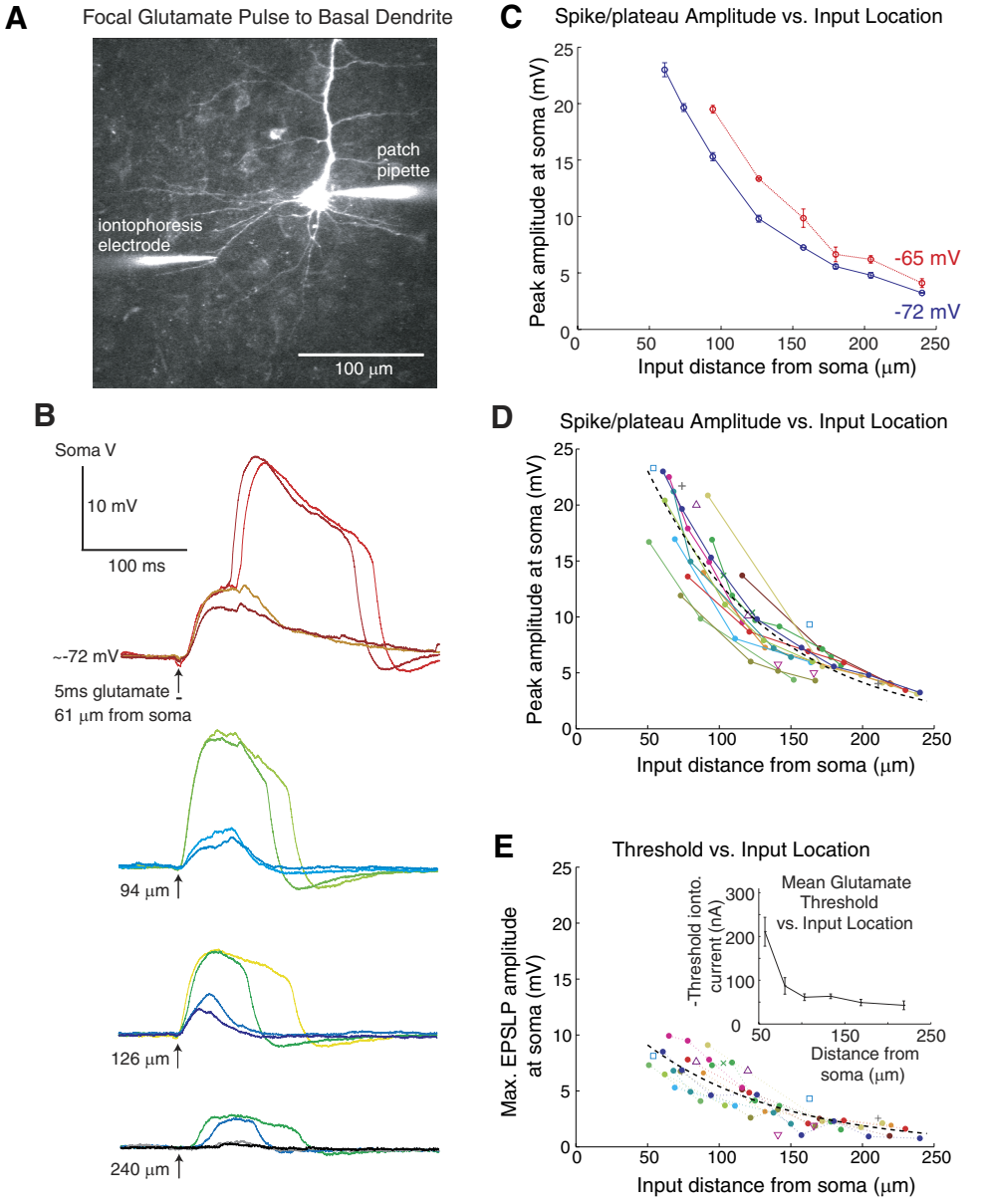

FIG. 1. Somatic amplitudes of basal dendritic spike/plateaus fall markedly with input distance from the soma. Glutamate iontophoresis data. *A*: experimental setup. A layer 5 neocortical pyramidal neuron is filled with the low-affinity calcium indicator Magnesium Green (K_d = 6 μM) via a whole cell patch pipette. A double-barreled sharp electrode with fluorescein in 1 barrel and glutamate in the other is advanced to within 1–2 μm of a basal dendrite. Mean projection of image stack taken with 2-photon microscope. *B*: a 5-ms pulse of glutamate is iontophoresed onto a basal dendrite at various distances from the soma (bigger iontophoretic currents indicated by "hotter" colors; different cell than *A*). Attenuated, smoothed voltage responses are recorded at the soma. Glutamate pulses above a threshold level evoke a spike/plateau potential in the dendrite, with an accompanying Ca^{2+} transient at the input site (see later figures). Spike/plateau amplitude, measured at the soma, decreases markedly from proximal to distal input sites. There is a similar drop in both voltage threshold (biggest subthreshold response) measured at the soma, and glutamate threshold. Baseline voltages (E_m) are within 1 mV of −72 mV and aligned. *C* and *D*: somatic amplitude of dendritic spike/plateaus vs. input location. *C*: same dendrite as in *B* (8 sites). Spike/plateau amplitude (mean ± SD) drops ~7-fold from proximal to distal and is bigger at −65 mV baseline E_m (red) than at −72 mV (blue). *D* and *E*: population data from 17 different Layer 5 pyramidal neuron terminal basal dendrites (n = 64 input sites). Points from a given dendrite are same color and symbol, with lines joining ≥3 sites from same dendrite. Baseline E_m −70 to −75 mV. Black dashed lines: exponential fits. *D*: spike/plateau amplitudes drop ~7.3-fold from proximal to distal, on average; functional length constant 87 μm. *E*: spike/plateau thresholds show similar proximal-to-distal drop. *Main plot*: peak amplitude at soma of largest subthreshold response versus input location; functional length constant 96 μm. *Inset*: mean glutamate threshold (iontophoretic current just sufficient to elicit a dendritic spike/plateau) vs. input location (n = 102 sites, bars = SE).

microscope. Small glutamate pulses, typically a few tens of nA or less, resulted in responses resembling slow-rising excitatory postsynaptic potentials, which we term excitatory postsynaptic-like potentials (EPSLPs; Fig. 1*B*). These grew in amplitude as the glutamate stimulus was increased. Above a threshold iontophoretic current, usually in the range 30–200 nA, there was a sudden jump in the somatic voltage transient as a spike/plateau initiated in the dendrite (Cai et al. 2004; Milojkovic et al. 2004, 2005a; Nevian et al. 2007; Polsky et al. 2004; Schiller et al. 2000; Wei et al. 2001). An attenuated, smoothed version of this spike/plateau was recorded at the soma (Figs. 1*B* and Supplementary S1). This event had a characteristic shape with a relatively fast onset and offset, separated by a slowly declining plateau in longer duration cases.

Each spike/plateau was associated with a pronounced, localized dendritic calcium transient, largely restricted to the stretch of the input dendrite close to the iontophoresis electrode (Supplementary Fig. S1; also see below; Schiller et al. 2000). Ca^{2+} transients associated with subthreshold EPSLPs were nearly always too small to be detected using Magnesium Green (see below and Supplementary Fig. S2). Typically no fluorescence transients were seen in neighboring dendrites, suggesting that the spike/plateau was restricted to the dendrite closest to the iontophoresis electrode. In a few cases where another dendrite crossed close by, or within ~10–20 μm of branch points, further increases in glutamate could evoke a second spike/plateau from the neighboring and/or parent dendrite with a further jump in somatic amplitude. A fluorescence transient was also then observed in the second dendrite (not shown). Such multi-dendrite responses were excluded from subsequent analysis.

Somatic amplitudes of dendritic spike/plateaus decrease strongly with input distance from the soma

When the iontophoresis electrode (or uncaging spot) is withdrawn gradually from a dendrite, the responses decrease sharply over a few micrometers; the cloud of glutamate ejected from the electrode reaches sufficient concentrations to activate NMDARs over a radius of ~10–25 μm, depending on the stimulus (Milojkovic et al. 2005a; Schiller et al. 2000; Major, unpublished data). NMDAR-dominated models predict that the spread of current to the soma from this zone of glutamate-bound NMDAR conductances near the input site will be determined largely by the passive electrical geometry of the cell with relatively little boosting by calcium or sodium conductances (Supplementary Fig. S3; Rhodes 2006; Schiller et al. 2000; Major, unpublished results). Between the input site and the tip, because of high local input impedance, the dendrite depolarizes to a voltage close to the glutamate reversal potential; however, the voltage falls off between the input site and the cell body (Milojkovic et al. 2004). As the input location is moved from the distal tip toward the proximal end of a terminal dendrite, NMDAR-dominated models predict that the zone of "active" (glutamate-bound) NMDAR conductance will slide along the dendrite and the amplitude of the plateau potential reaching the soma will grow. This will be true as long as distal-to-proximal propagation of voltages along the dendrite is nonregenerative. What the models cannot predict a priori is whether there is sufficient NMDAR conductance to support a spike/plateau at all locations in real basal dendrites. Also the proximal-to-distal gradient in somatic amplitudes is highly dependent on parameters such as specific membrane resistance R_m and cytoplasmic resistivity R_i.

A major finding of this study is that the spike/plateau amplitude at the soma can increase more than sevenfold as the input site is moved from distal to proximal along a given terminal basal dendrite. In a representative example, the spike/plateau amplitude at the soma grew from 3.2 to 23 mV as the input site was moved proximally along the dendrite from 240 to 61 μm away from the soma (Fig. 1, *B* and *C*).

When the soma was depolarized, a similar progression in amplitudes was observed but the amplitudes were larger, in line with increases in input resistance (Figs. 1*C* and Supplementary S2, *B1, D1,* and *D3*). To reduce scatter due to this inward rectification, we compared iontophoretic responses across input sites and cells over a restricted range of baseline membrane potentials, between −75 and −70 mV. We reiterate that only spike/plateaus originating from a *single* terminal dendritic segment were included in this analysis. We further confined our amplitude-distance analysis to spike/plateaus with a relatively narrow range of durations (50–100 ms), where possible. This ensured that responses were clearly suprathreshold but reduced scatter due to any slight additional growth in amplitude seen with further increases in glutamate (Supplementary Fig. S2, *A1* and *C1*).

There was a consistent and striking spatial gradient in spike/plateau amplitude for all the dendrites tested ($n = 64$ input sites, 17 terminal basal dendrites, 17 cells; Fig. 1*D*). The mean spike/plateau amplitude at the soma was 20.6 ± 2.8 (SD) mV for proximal inputs and 3.85 ± 0.55 mV for distal inputs, significantly smaller (50–70 vs. 200–240 μm from soma, $n = 7$ and 8, $P < 10^{-9}$). The population data were least-squares fitted with a decaying single exponential to estimate a "functional length constant"—not to be confused with the passive electrotonic space constant of an infinitely long unbranched cable (Rall 1977). The fall-off with distance had a functional length constant of ~87 μm (95% confidence interval or CI, 77–100 μm). The fitted amplitude was 23 mV at 50 μm from the soma, the most proximal location. The most distal spike/plateaus were 3.1–3.2 mV in amplitude, 7.3-fold smaller.

The somatic amplitudes of the largest just subthreshold EPSLPs showed a similar spatial gradient to the spike/plateaus (Fig. 1*E*). The functional length constant of this fall-off was 96 μm (CI, 80–119 μm) with the best-fit somatic voltage amplitude ranging from 9.1 mV down to 1.3 mV as the input site moved from 50 to 240 μm away from the soma, a sevenfold drop.

The glutamate threshold for spike/plateau initiation also showed a fall-off with distance from the soma, despite calibration uncertainties and considerable scatter (see Supplementary material). The mean iontophoretic current required to just elicit a dendritic spike/plateau dropped 4.9-fold from −210 ± 32 (SE) nA proximally to −43 ± 10 nA distally (Fig. 1*E, inset,* $n = 102$ locations).

Amplitude versus location experiments performed using single photon uncaging of MNI glutamate yielded similar results (Fig. 2; $n = 9$ dendrites, 34 locations). At baseline membrane potentials of −75.3 ± 9.1 (SD) mV, spike/plateau amplitudes fell off strongly with input distance from the soma, with a functional length constant of 77 μm (CI, 67–91 μm).

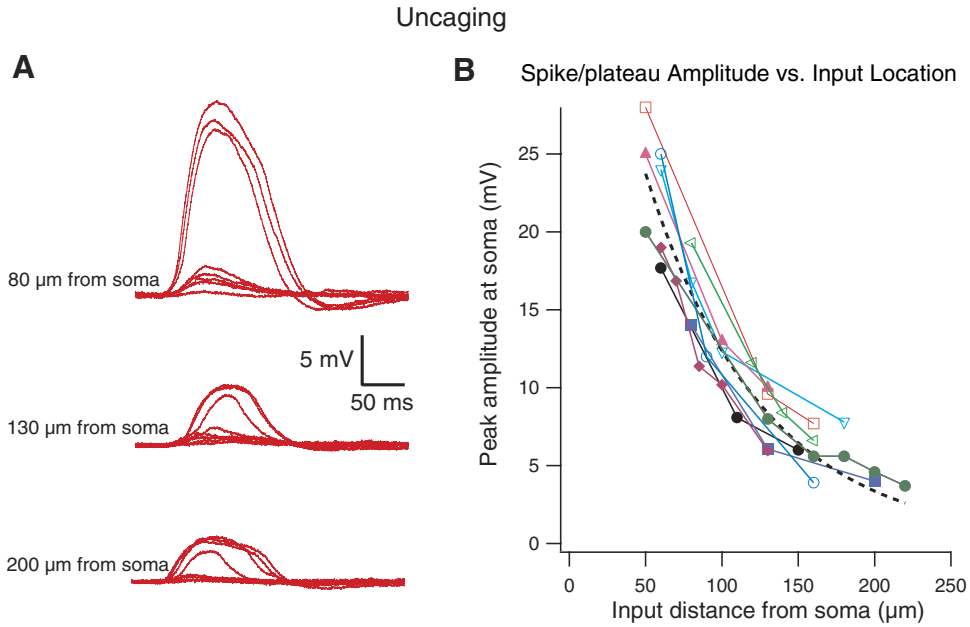

FIG. 2. Somatic amplitudes of basal dendritic spike/plateaus fall markedly with input distance from the soma. UV glutamate uncaging data. *A*: excitatory postsynaptic-like potential (EPSLP) and spike/plateau responses evoked in the presence of MNI-glutamate by increasing laser intensities at 3 locations along a basal dendrite of a layer 5 pyramidal neuron (~1-ms pulses 80, 130, and 200 μm from soma). Responses all recorded at soma. Note the large decrease in spike/plateau amplitude as the stimulation moved from proximal to distal locations. *B*: summary plot showing the total amplitude of the spike/plateau as a function of distance for 9 dendrites. Points from same dendrite have same color and symbol and are connected by a line. Black dashed line: exponential fit, functional length constant 77 μm.

Spike/plateau amplitudes ranged from 24.3 ± 4.0 mV at 50 μm to 3.7 mV at 220 μm, a 6.6-fold reduction.

Basal dendritic spike/plateaus are NMDAR-dominated, irrespective of input location

We explored the ionic basis of the spike/plateaus over the full range of terminal basal dendritic input locations and somatic amplitudes (Fig. 3). Responses were divided into proximal and distal groups (50–100 μm, Fig. 3, *left*, and 100–200 μm from soma, *right,* respectively). In all cases, calcium channel blockers (100 μM Cd^{2+} plus 100 μM Ni^{2+}) had only minor effects on the spike/plateau (Fig. 3, *A* and *B2;* positive controls discussed in Supplementary material). Proximal spike/plateau amplitudes barely changed, from 19.6 ± 5.2 mV (control) to 18.6 ± 5.9 mV in Cd^{2+}/Ni^{2+} ($n = 7$, $P = 0.2$, paired *t*-test). Likewise, amplitudes of distal spike/plateaus barely changed from 7.0 ± 2.7 mV (control) to 7.7 ± 3.4 mV in Cd^{2+}/Ni^{2+} ($n = 8$, $P = 0.15$). The amplitude of the biggest just-subthreshold EPSLP measured at the soma was taken as a measure of threshold (as in Fig. 1*E*). Thresholds of proximal spike/plateaus rose from 4.6 ± 1.0 to 6.4 ± 1.6 mV in Cd^{2+}/Ni^{2+} ($n = 9$, $P = 0.05$). Thresholds of distal spike/plateaus rose slightly from 1.9 ± 0.5 (control) to 3.1 ± 2.0 mV ($n = 8$, $P = 0.11$). Comparable results were found with iontophoresis experiments (not shown).

Application of the Na^+ channel blocker TTX (1 μM) had only minor effects on spike/plateaus (Fig. 3, *E1* and *G*). Proximal amplitudes barely changed from 24.4 ± 4.6 (control) to 24.5 ± 5.1 mV in TTX ($n = 7$, $P = 0.98$). Distal spike/plateau amplitudes fell ~15%, from 8.7 ± 3.8 to 7.4 ± 3.8 mV ($P = 0.0007$; $n = 12$). On average, thresholds of proximal spike/plateaus increased slightly from 9.3 ± 3.0 to 11.4 ± 3.5 mV in TTX ($P = 0.23$); thresholds of distal spike/plateaus averaged 2.1 ± 1.2 mV (control) and 1.8 ± 1.1 mV in TTX ($P = 0.13$). In cases where the spike/plateau had a very rapid onset and/or was preceded by a small fast spikelet (Milojkovic et al. 2005b), these were abolished by TTX with minimal changes to the underlying plateau.

By contrast, 100 μM APV +10 μM MK801 completely abolished the spike/plateaus (Fig. 3, *A, 1* and *2,* and *B, 1* and *2*), so that, unlike in calcium and sodium channel blockers, they could not be re-initiated at higher stimulus levels. This was consistently found over the entire range of input locations and spike/plateau amplitudes tested (50–200 μm from soma, $n =$ 10 proximal, $n = 5$ distal, amplitudes: 4–36 mV).

Calcium-activated nonspecific cation conductances (Wang et al. 2006) are unlikely to have made a significant contribution as chelating intracellular calcium with bis-(*o*-aminophenoxy)-*N,N,N′,N′*-tetraacetic acid (BAPTA) did not significantly change the spike/plateau in layer 5 basal dendrites (Gordon et al. 2006) and in CA1 apical tufts/obliques actually prolonged spike/plateaus rather than shortening them (Wei et al. 2001). Similarly, excessive intracellular perfusion with the high-affinity indicator Calcium Green-1 abolished basal dendritic spike/plateau-associated calcium transients without blocking the spike/plateau itself (>1 h whole cell recording, not shown).

Local dendritic spike/plateaus are accompanied by a large calcium transient at the input site with a smaller calcium transient extending to the dendritic tip

NMDAR-dominated models predict that the high calcium zone associated with a spike/plateau will move with the input location along a dendrite. Because the dendrite is depolarized all the way from the input site to the distal tip, if there is a minor contribution from voltage-activated calcium conductances (Schiller et al. 2000), these models also predict there will be a smaller calcium transient throughout the dendrite distal to the high-Ca^{2+} zone.

These predictions were confirmed by two-photon calcium imaging. Calcium profiles were computed from the medians of multiple trials taken at various focal planes and positions along the dendrite. In an example case, a proximal spike/plateau lasting ~150 ms was evoked in a basal dendrite 68 μm from the cell body (Fig. 4, *A–C,* Magnesium Green, line scans). At the input site, there was a large calcium transient,

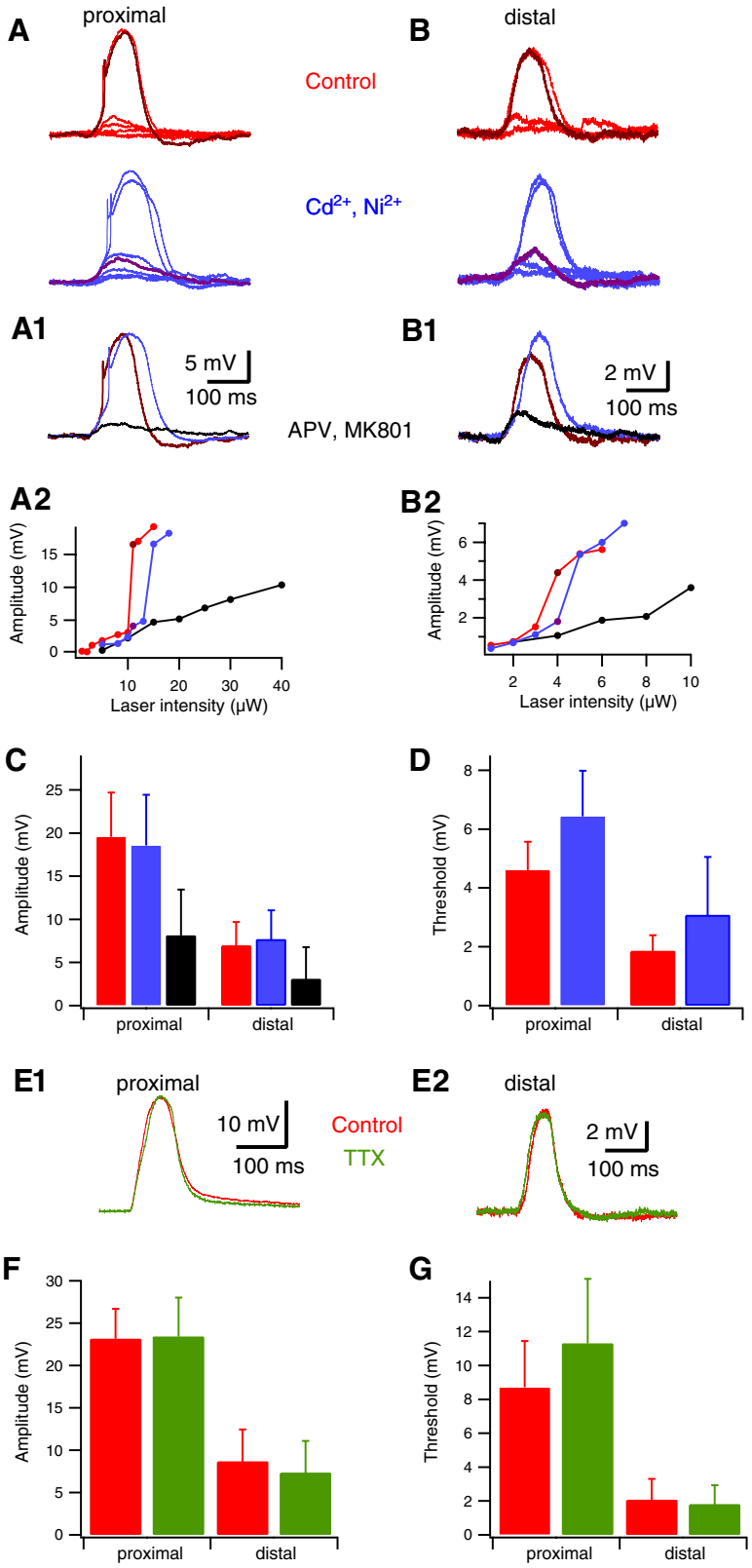

FIG. 3. Spike/plateaus are *N*-methyl-D-aspartate receptor (NMDAR) conductance-dominated at all basal dendritic input locations with minor contributions from Ca^{2+} and Na^{+} conductances. *A*: UV uncaging responses (~1-ms pulses) in MNI-glutamate were evoked at increasing laser intensities on a basal dendrite 60 μm from the soma in control conditions (red) and in the presence of 100 μM Cd^{2+} +100 μM Ni^{2+} (blue). Note small sodium spikelet at leading edge. Thick brown and purple traces at stimulus intensity just giving spike/plateau in control (subthreshold in Cd^{2+} + Ni^{2+}). *A1*: overlay of the spike/plateau in control condition (brown) and in Cd^{2+} + Ni^{2+} (blue, bigger stimulus). The spike/plateau response was completely blocked by 100 μM 2-amino-5-phosphonovaleric acid (APV) +10 μM MK801 (black) and could not be reinitiated at higher stimulus intensities. *A2*: peak voltage response at increasing laser intensity for control (red), Cd^{2+} + Ni^{2+} (blue), and APV + MK801 (black). Note that in Cd^{2+} + Ni^{2+}, a full-blown dendritic spike/plateau can be re-initiated with a slight increase in both the threshold stimulus and peak somatic voltage of the largest just subthreshold response. *B*: equivalent data for input 130 μm from soma. *C* and *D*: summary of the peak response amplitudes and thresholds at the soma, respectively, under control conditions, Cd^{2+} + Ni^{2+}, and APV + MK801 for proximal locations (50–100 μm from soma) and distal locations (100–200 μm from soma). The threshold was defined as the amplitude of the largest subthreshold EPSLP before a spike/plateau initiated, measured at the soma. *E1*: overlay of spike/plateau under control conditions (red) and during 1 μM TTX application (green). Input 90 μm from soma. *E2*: equivalent data for input 140 μm from soma, different dendrite. *F* and *G*: summary of the peak response amplitudes and thresholds at the soma, respectively, under control conditions, and TTX.

rising during the voltage plateau, exhibiting some "flat-topping" then falling after a delay—consistent with indicator saturation (see below; compare with Milojkovic et al. 2007). Proximal to the input site, the fluorescence transient extended ~20 μm with a delayed rise at more proximal locations. Distal to the input site, the peak transient dropped over ~30–40 μm before leveling off and continuing to the dendritic tip at a $\Delta F/F$ significantly above the background noise. In this lower-Ca^{2+} distal zone, the transient rose during the voltage plateau, then began to fall immediately

afterward and exhibited minimal saturation with this indicator.

The high-Ca^{2+} zone did indeed follow the iontophoresis electrode along a given dendrite (e.g., Fig. 4*C*, red starred profiles) and always peaked within a few microns of the point closest to the electrode tip. High-Ca^{2+} zones typically had half-widths of the order of 20–40 μm for spike/plateau durations in the range 75–160 ms (Fig. 4*C*). The high-input site, lower distal zone profile of Ca^{2+} transients was qualitatively very reproducible ($n = 9$ basal dendrites, 11 input sites). A similar pattern was also observed in apical oblique dendrites ($n = 2$, example in Fig. 4*C*).

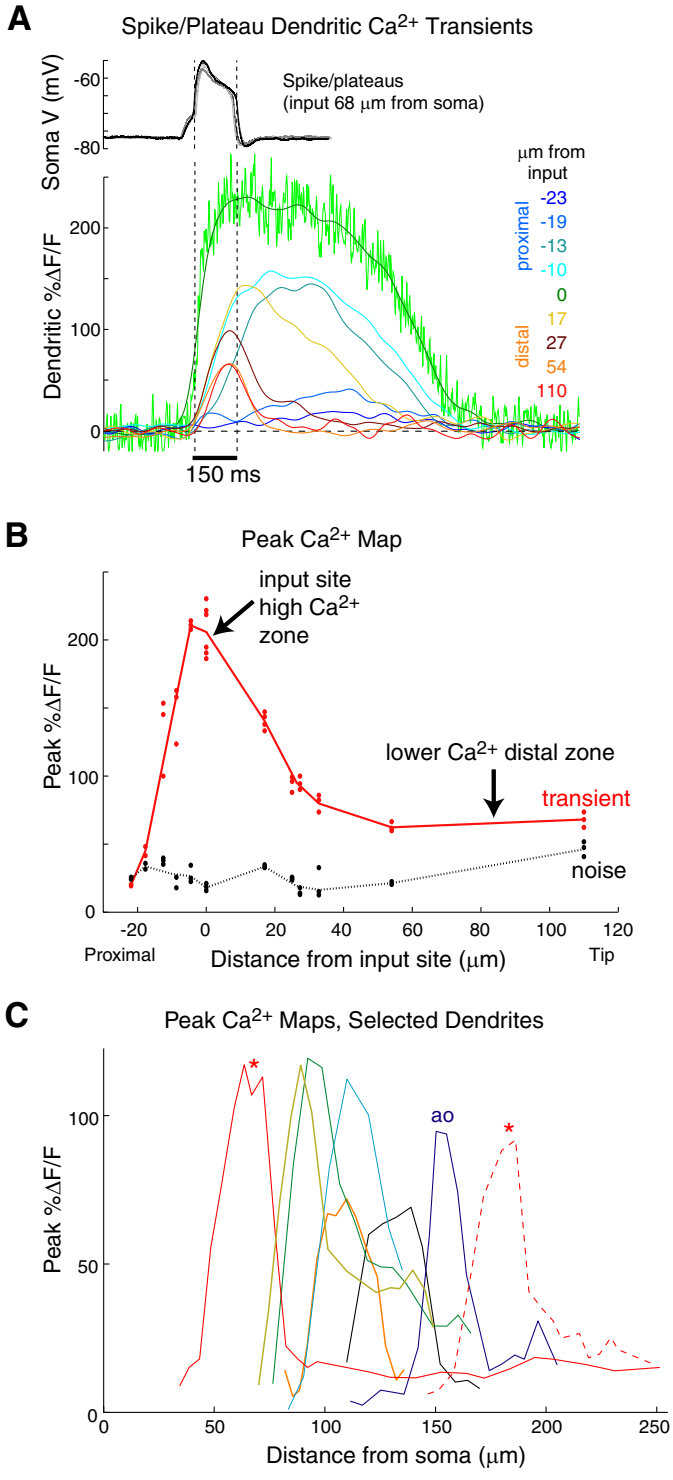

Spike/plateau duration grows with increasing glutamate and depolarization

Consistent with previous reports (Milojkovic et al. 2005a; Nevian et al. 2007), we found that while the amplitude of the spike/plateau is predominantly all or none at a given location, the duration (and hence the time integral) increased progressively and substantially with the glutamate stimulus (examples in Figs. 1*B*, 2A, 5*A*, and 6*A*). The iontophoretic current required to produce a spike/plateau of a given duration varied across input sites (see Supplementary material), so to pool data, we normalized the iontophoretic current by I_{100ms}, the current yielding a "standard " plateau duration of 100 ms. The mean increase in duration across a representative sample of eight dendrites was 82 ms/I_{100ms} (CI, 73–90; Fig. 5*B*). On average, a 12-fold increase in iontophoretic current led to a more than fivefold growth in plateau duration (increasingly sublinear at higher glutamate currents). Spike/plateaus also grew in duration with depolarization; the mean increase across a representative sample of 10 dendrites was 1.07 ms/mV (CI, 0.85–1.29 ms/mV; Fig. 6*C*). A 20-mV depolarization would therefore nearly double the duration of a spike/plateau at the briefer end of the spectrum. This represents a potential mechanism for spike/plateaus at different locations to interact cooperatively.

Fluorescence transient saturates at the input site as glutamate increases

The fluorescence transients in Fig. 4*A* were associated with a relatively long NMDA plateau, of duration ~150 ms,

FIG. 4. Basal dendritic spike/plateaus are accompanied by a large calcium transient near the input site and a smaller transient extending to the dendritic tip. *A, top*: somatic voltage recording of basal dendritic spike/plateau evoked 68 μm from soma. Several traces (different gray shades), with baselines aligned (shifts < 1 mV) to show consistency. Black dashed vertical lines indicate duration of plateau. *Bottom*: calcium transients (Magnesium Green, low-affinity calcium indicator) at various distances from the input site. Line scan, 2-ms line time. Light green, smoothed with Gaussian of SD 10 ms; other traces, SD 40 ms. Distances of region of interest (ROI) centers from electrode tip are indicated (negative distances are proximal to electrode). Peak fluorescence change drops to noise levels over ~20 μm proximally and falls off within 30 or 40 μm distally, then remains more or less constant the rest of the way to the tip of the dendrite. *B*: composite map of peak relative fluorescence change vs. distance from input site. Red: calcium transient; black: 95% confidence interval for baseline noise. Dots: values from individual traces. Line: median values. Only in-focus regions analyzed. There is a high calcium zone at the input site and an approximately uniform distal lower calcium zone extending to the dendritic tip. *C*: high calcium zone tracks input location; multiple high calcium zones can fit within a single dendrite. Ca^{2+} maps of dendritic spike/plateaus (duration, 75–160 ms) from different dendrites plotted with respect to distance from soma ($n = 8$). Peak coincides with input site in all cases. A given color and line-style indicates a particular dendrite and input location. Red plots (*) are from proximal and distal input sites of same dendrite as in Fig. 1, *B* and *C* (plateau durations from 90 to 130 ms and from 90 to 110 ms, respectively). Dark blue solid line (ao): data from an apical oblique dendrite. The characteristic pattern of a high calcium zone at the input site, a fairly uniform distal zone of lower calcium, and rapid fall-off proximal to the input site was consistent across all dendrites and input sites (and a wide range of stimulus strengths, not shown).

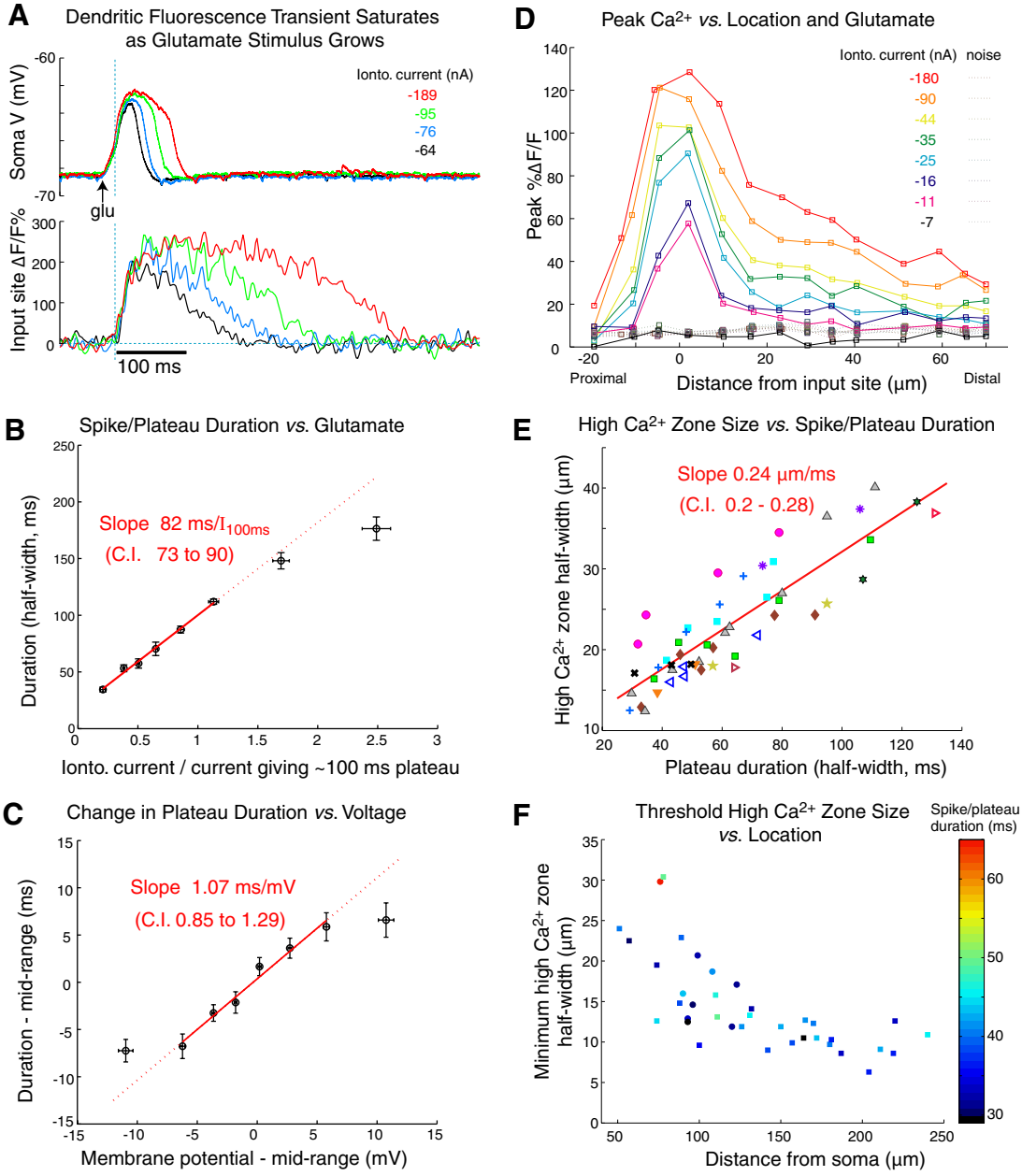

FIG. 5. Input site high calcium zone grows with glutamate and spike/plateau duration. Threshold high calcium zone size increases from distal to proximal. *A*: fluorescence transients near input site saturate as glutamate stimulus increases (input 187 μm from soma). *Top*: spike plateau duration increases with glutamate. *Bottom*: brief (~30 ms) NMDA spikes are associated with an input site fluorescence transient that rises during the depolarization then falls afterward (Magnesium Green, low-affinity calcium indicator). As the stimulus increases and the spike/plateau duration grows, the fluorescence shows progressive signs of saturation, rising then leveling off during the spike/plateau, and remaining at a roughly constant level for a period after the spike/plateau, before falling again. The maximum level is similar over a wide range of stimuli; the time spent at this level increases with stimulus strength. *B*: spike/plateau duration increases with glutamate stimulus. Population data, at baseline membrane potentials between −60 and −70 mV. For each input site, glutamate normalized by I_{100ms}, the iontophoretic current giving ~100-ms plateau (n = 8 dendrites, 7 cells, total of 10 duration-glutamate relations pooled at different E_m's). Red line, linear regression (dotted = extrapolation). *C*: spike/plateau duration increases with depolarization, population data. Changes in duration vs. membrane potential relative to mid-range explored for each site (data from different input sites and cells were approximately parallel but offset lines, not shown; n = 10 dendrites, 9 cells, total of 27 duration-voltage relations pooled for different iontophoretic currents). Red line, linear regression (dotted = extrapolation). *D*: high calcium zone grows with strength of glutamate pulse. Calcium maps (Magnesium Green) show graded increases with size of glutamate pulse. Maps of peak relative fluorescence change vs. distance from input site for different iontophoretic pulse amplitudes I_{ionto} (duration, 5 ms), for a single basal dendritic input site 96 μm from soma. Median peak transients indicated by solid lines, 95% confidence interval of baseline noise by darker dotted lines. As the stimulus increases, the high calcium zone grows both in spatial extent and amplitude (the latter showing saturation). Amplitude of peak Ca^{2+} transient in distal zone also increases with stimulus, but more linearly. Black (lowest) trace from biggest just subthreshold EPSP-like response—no Ca^{2+} transient was detectable. *E*: high calcium zone increases in size with plateau duration. Zone half-width vs. duration of spike/plateau. Different colors/symbols indicate different input sites; red line, linear regression on all points; C.I., 95% confidence interval. Rectangle scans, 64 ms per time point (14 input sites mapped). *F*: threshold high calcium zone size decreases with distance from soma. Half-width just above NMDA spike threshold vs. input location; colors indicate duration (n = 37 input sites, squares = square frame scans, circles = rectangle scans).

and showed signs of saturation at the input site even though the affinity of the calcium indicator was low, $K_d \sim 6$ μM. By contrast, when brief just-suprathreshold NMDA spikes were elicited, the fluorescence transients showed little saturation, falling soon after the end of the spike, and reaching baseline within a few hundred milliseconds (Fig. 5*A*). As the stimulus was increased, fluorescence saturation with flat-topping became progressively more evident. The saturated level in many cases continued after the end of the spike/plateau (e.g., red traces), and the fluorescence transient took progressively longer to fall to baseline (compare with Milojkovic et al. 2007).

High-calcium zone grows with increased glutamate and spike/plateau duration

The input site high-calcium zone grew in amplitude and extent as the glutamate pulse and the spike/plateau duration increased ($n = 11$ dendrites; representative example in Fig. 5*D*). In the distal zone, the calcium transient also grew in amplitude ($n = 8$ dendrites), the increase being more linear with plateau duration than near the input site, consistent with less indicator saturation ($n = 3$ dendrites). There was a particularly striking approximately linear correlation between spike/plateau duration and high-calcium zone size (half-width or width at half-maximal $\Delta F/F$ amplitude, slope 0.24 μm/ms, $n = 14$, Fig. 5*E*; plotting zone size vs. various normalized measures of iontophoretic current resulted in more scatter).

High-calcium zone size at NMDA spike threshold falls from proximal to distal input locations

As reported above, there was a strong spatial gradient in both glutamate threshold and maximal just-subthreshold response at the soma, and a similar gradient was seen in the threshold NMDA conductance required to support NMDA spikes in compartmental models (see below). There was no consistent spatial gradient in the minimum duration of just-suprathreshold NMDA spikes [Fig. 5*F*, colors; 38.4 ± 7.1 (SD) ms]. However, the high-calcium zone half-widths associated with just suprathreshold NMDA spikes did fall off with distance from the soma, from ~25 μm proximally to ~10 μm distally. Grouping the data into three distance bands gave the following mean half-widths: 18.8 ± 6.5 (SD) μm (≤100 μm from soma), 13.1 ± 2.8 μm (100–170 μm), and 9.9 ± 1.9 μm (≥170 μm; $P = 0.0076$ and 0.0055 between neighboring groups; $P = 0.0004$ between proximal and distal).

Depolarization reduces glutamate thresholds of NMDA spike/plateaus with an approximately linear trade-off

To test the effect of depolarization on NMDA spike initiation, the input-output relationship at single basal dendritic sites was explored by applying brief glutamate pulses of different amplitudes at various baseline membrane potentials E_m under somatic current clamp (Figs. 6 and Supplementary S2). At each membrane potential, there was a clear glutamate threshold below which the voltage response at the soma resembled a slow excitatory postsynaptic potential and above which a spike/plateau potential was generated accompanied by an obvious local Magnesium Green-fluorescence transient. As the cell was hyperpolarized, the glutamate threshold increased; as it was depolarized, the glutamate threshold decreased (Figs. 6*A* and Supplementary S2*A*). The change in glutamate threshold with E_m was substantial; in this example, only half as much iontophoretic current was required to trigger a spike/plateau at −66 mV than at −83 mV. A similar finding was reported in apical tufts/obliques of CA1 pyramidal neurons in organotypic slices (Wei et al. 2001, their Fig. 2*B*), although the amplitudes of their responses increased with hyperpolarization, not depolarization, and they increased the duration of their glutamate pulses not the amplitude during glutamate threshold tests.

Likewise, with the exception of larger pulses, for each size of glutamate pulse leading to a spike/plateau, there was a clear "prevention threshold" or baseline somatic membrane voltage below which the spike/plateau was not generated and above which it was (Figs. 6*B* and Supplementary S2, *B* and *D*). It should be noted that the prevention voltage was measured at the soma and would not be the same as the actual voltage threshold for spike/plateau initiation at the dendritic input site. The bigger the glutamate pulse, the more the neuron needed to be hyperpolarized to prevent the spike/plateau. In the example shown, the prevention threshold was approximately −69 mV for a −42 nA × 5-ms glutamate iontophoretic pulse and approximately −84 mV for a −89-nA pulse (Fig. 6*B*). The prevention threshold for the calcium transient at the input site was always the same as for the voltage spike/plateau (Supplementary Fig. S2*B*). At most input sites tested, glutamate pulses beyond a certain size resulted in spike/plateaus that were not preventable by hyperpolarization down to −100 mV.

Glutamate and depolarization interacted approximately additively, to within a scale factor, in determining whether a response was sub- or suprathreshold in the dendrite. The local spike/plateau mechanism had a negatively sloped, approximately linear threshold boundary in the two-dimensional glutamate-voltage space explored (Fig. 6, *C* and *D*): depolarization trading off approximately linearly with glutamate. (Glutamate, voltage) combinations to the bottom-left of the threshold line produced subthreshold EPSLPs, whereas (glutamate, voltage) combinations to the top-right led to spike/plateaus. The mean gradient of the threshold line for a representative sample of 11 input sites was −4.4% per mV (CI, −5.4 to −3.4; normalizing by the mid-range of iontophoretic currents used at each site and aligning on the mid-range of voltages explored).

In principle then, depolarization from a spike/plateau could indeed facilitate other spike/plateaus elsewhere in the neuron, in particular in the proximal part of the same dendrite, which will experience a bigger voltage swing than other dendrites. This facilitation will take two forms: assisting threshold crossing and prolongation of duration. Every millivolt of depolarization propagating from the first spike/plateau to a second location would be predicted to reduce the glutamate threshold for a plateau at the second location by ~4% on average. The duration of an already suprathreshold plateau at the second location would be predicted to increase by ~1 ms/mV of "baseline" depolarization at that site (i.e., per mV propagating to the 2nd site in the absence of any inputs there; Fig. 5*C*).

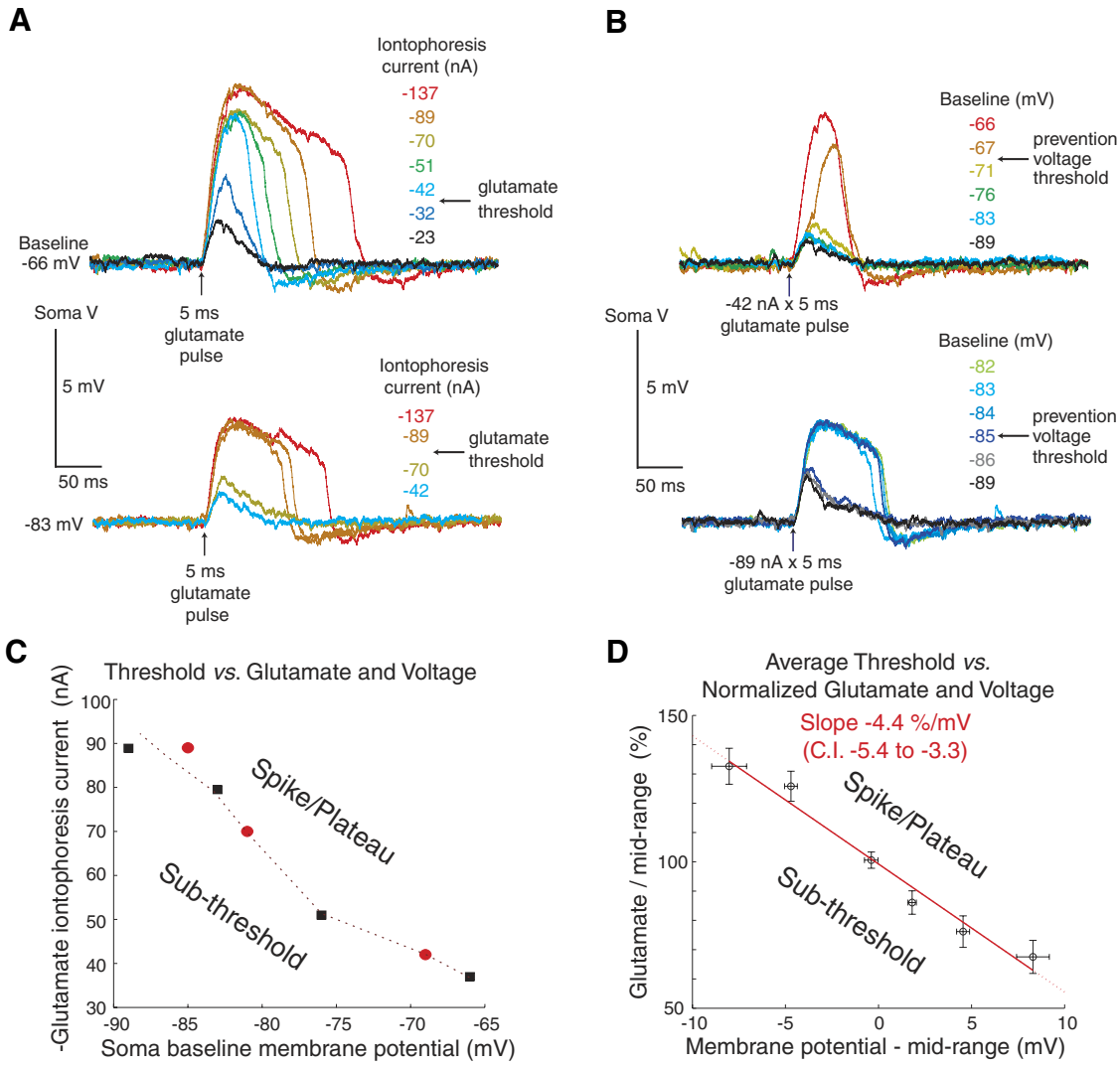

FIG. 6. Spike/plateau thresholds exhibit approximately linear trade-off between glutamate and depolarization. *A–C*: responses at soma from stimulating a representative input site on a basal dendrite; iontophoresis electrode 215 μm from the soma. *A*: spike/plateaus have voltage-dependent glutamate thresholds. Hotter colors indicate larger glutamate pulses; traces within 1 mV of indicated somatic membrane potentials (E_m), offset to align baselines. Depolarization (*top traces*) decreases the glutamate threshold, hyperpolarization (*bottom traces*) increases it. *B*: each glutamate pulse above a certain size is associated with a somatic baseline voltage above which the pulse triggers a dendritic spike/plateau and below which it only elicits an EPSLP. The larger the glutamate pulse, the more negative this "prevention voltage threshold." Colder colors indicate more hyperpolarized; baselines aligned. *C*: spike/plateau threshold in 2 dimensions with respect to glutamate and baseline somatic E_m. *Black*, thresholds from glutamate threshold tests (*A*, Supplemental Fig. S2*A, 1* and *2*). *Red*, thresholds from prevention voltage threshold tests (*B,* Supplemental Fig. S2*B, 1* and *2*). *Dotted line*: threshold line, i.e., boundary between regions of the parameter space producing subthreshold EPSLPs (*bottom left*) and supra-threshold spike/plateaus (*top right*). *D*: threshold vs. glutamate and baseline somatic E_m: population data (n = 11 input sites, 8 dendrites, 7 cells, means ± SE). For each input site, glutamate is normalized by mid-range of iontophoretic currents explored and voltage is measured relative to mid-range of membrane potentials explored. (Glutamate, voltage) combinations top/right of red best-fit line produced spike/plateaus. Glutamate and baseline voltage trade off approximately linearly, i.e., interact approximately additively, to within a scale factor, in determining whether response is suprathreshold in the dendrite.

Proximal-to-distal drop in local input conductance is key to the fall-off in plateau amplitudes

Both the average glutamate threshold for dendritic spike/plateau initiation and the maximum just-subthreshold EPSLP at the soma also decrease by large factors with input distance from the soma (5- and 7-fold, respectively; Fig. 1*E*). We simulated basal dendrite behavior using detailed compartmental models (Carnevale and Hines 2006) based on the morphology of a reconstructed and measured layer 5 pyramidal cell (Larkman et al. 1992); see Supplementary material. For simplicity, because of the evidence that the dendritic spike/plateaus are dominated by NMDAR conductances (see below), we included no other active conductances and constrained the passive membrane time constant and specific membrane capacitance to experimentally determined values (Major et al. 1994; Mason and Larkman 1990; Trevelyan and Jack 2002). The observed spread of spike/plateau amplitudes could be reproduced by setting cytoplasmic resistivity to 100 Ωcm in more proximal dendrites and 120 Ωcm in thinner distal dendrites (Supplementary Fig. S3). A robust feature of this and other models that reproduce the observed spatial gradient in spike/plateau amplitudes (including those with active conductances, not shown), is that around six- to sevenfold more NMDA conductance and

current is needed to initiate a proximal than a distal spike/plateau. The reason for this is that as the input site moves from the proximal end of a terminal dendrite, near other branches and the soma, to the more isolated distal tip (sealed end), the local input conductance falls by a similar factor (Nevian et al. 2007; Rhodes 2006). For example, the local input conductance falls 6.5-fold, from 11 to 1.7 nS in the case of the passive model in Supplementary Fig. S3. Proportionately less NMDAR conductance is required to make the distal part of the dendrite bistable (Supplementary Fig. S4; Schiller and Schiller 2001). Because most of the NMDAR current flows proximally down the dendrite via the soma to the rest of the cell, the most proximal plateau causes an approximately sevenfold bigger somatic voltage swing than the most distal plateau.

DISCUSSION

At the outset of this study we had a number of questions. Can all parts of a basal dendrite support a spike/plateau? Are there any differences between proximal and distal spike/plateaus, in terms of input-output relations (thresholds, amplitudes, durations) or underlying ionic conductances? What fraction of the dendrite is required to support an NMDA spike, and how does this vary from proximal to distal? Can different parts of one or more dendrites interact co-operatively?

Basal dendritic spike/plateaus have a sevenfold spatial gradient in somatic amplitude and a high calcium zone at the input site

Focal glutamate stimuli can generate local spike/plateau potentials in single terminal basal dendrites of large Layer 5 cortical pyramidal neurons. The main finding of this study is that there is, on average, a smoothly graded ~7-fold increase in the spike/plateau amplitude reaching the soma as the input site is moved inward along a terminal basal dendrite from the distal tip to 50 μm from the soma. (We exclude spike/plateaus originating from more than one dendritic segment, near branch points or where dendrites cross close to one another). Another finding is that focally-evoked local spike/plateaus are accompanied by a characteristic pattern of dendritic calcium transients. There is a high calcium zone within 5 to 20 μm of the input site, rapid fall-off proximal to the input site, and a roughly uniform zone of lower calcium extending to the distal tip (compare with Milojkovic et al. 2007). Both the distance dependence and the two calcium zones are consistent with an ionic mechanism dominated by localized activation of NMDAR conductances in the dendritic cable (Schiller et al. 2000).

Spike/plateaus are NMDAR-conductance dominated at all basal dendritic locations

Prior to this study it was not clear whether very proximal spike/plateaus could be evoked, and, if so, whether they were NMDAR-dominated. An important finding of this study is that blockade of calcium and/or sodium channels has relatively minor effects on basal dendritic spike/plateaus at *all* input locations tested - although both glutamate and voltage thresholds rise (in most cases). By contrast, blockade of NMDARs totally abolishes the spike/plateaus, consistent with NMDAR conductances dominating the total current flowing during these events.

There are several other lines of evidence pointing toward NMDA receptor currents being the dominant contributors to total charge flow during basal dendritic spike/plateaus in neocortical pyramidal neurons:

a) the steep drop-off in amplitudes at the soma with input distance, implying the spike/plateaus do not propagage regeneratively toward the soma; the dendritic membrane cannot therefore have densities of sodium or calcium channels high enough to generate a bistable local current-voltage relation which could support local initiation of a spike/plateau in the absence of NMDAR conductances.

b) the graded increase in duration with stimulus strength,

c) the input site high calcium zone and distal lower calcium zone (see below),

d) the inability of local dendritic current injection $\leq$140 μm from the soma to evoke calcium spikes (Nevian et al. 2007) (fast local sodium spikes can be triggered only in ~1/3 of cases 50–100 μm from the soma, but not from 100–140 μm away), and

e) simulation results (Rhodes 2006; Schiller et al. 2000).

Taken together with the pharmacology, these findings show that under our experimental conditions NMDAR conductances dominate local basal dendritic spike/plateaus in neocortical pyramidal neurons, whereas calcium and sodium conductances play a subsidiary role.

Together, sodium and calcium conductances may still play an important role, because they can sharpen thresholds and enable dendritic spike/plateau generation at lower levels of NMDAR conductance (i.e., fewer activated synapses), which also allows for briefer just supra-threshold responses (Schiller et al. 2000). In some cases sodium conductances are also responsible for a spikelet or rapid rise on the leading edge of the spike/plateau (seen in ~18% of cases when recorded at soma, e.g., Figure 3*A*, and ~40–75% of cases recorded in the dendrite with voltage-sensitive dyes; Milojkovic et al. 2005b). There are other possible caveats. For example, sodium and calcium channels may have more influence on dendritic computations during network activity, for example back-propagating action potentials may help trigger dendritic spike/plateaus. Rapidly-inactivating sodium and calcium channels may play more of a role in response to extremely rapidly-rising glutamate transients from synchronous inputs (Losonczy and Magee 2006), especially if ambient glutamate levels turn out to be sub-micromolar (Cavelier et al. 2005), favoring AMPA receptor over NMDAR activation - for example, if network activity is sparse (Shoham et al. 2006). Also, neuromodulators and homeostatic processes may change the relative influences of different dendritic conductances (Davis 2006; Seamans and Yang 2004).

Calcium profiles

The simplest explanation for the observed pattern of a high calcium zone around the input site and a lower calcium zone distally (Figs. 4 and 5) is that there is a dynamic zone of '*active*' NMDAR conductance around the input site and a much lower density of calcium channels throughout the dendrite. Here 'active' means binding both glutamate and co-agonist (D-serine or glycine; Wolosker 2007), and therefore

behaving as a depolarization-activated conductance. We suggest that the active NMDAR conductance density falls off over a few tens of microns, depending on the size of the glutamate pulse and the spatiotemporal concentration profile of the expanding cloud of glutamate (see below for discussion of Ca^{2+} diffusion). This profile of active NMDAR conductance is consistent with the decline in the response as the electrode or uncaging spot is moved away from the dendrite (Milojkovic et al. 2005a; Schiller et al. 2000). Charge flowing through the active NMDAR conductance zone depolarizes the dendrite near the input site. This depolarization propagates to the dendritic tip, largely passively, opening sodium and calcium channels present in the membrane at a density too low for significant regenerative propagation toward the soma. The result is the relatively uniform pattern of lower calcium influx in the distal zone, which terminates as soon as the spike/plateau repolarizes, and the rapid fall-off in calcium entry proximal to the input site. Calcium release from internal stores has been shown not to play an important role in basal dendritic spike/plateau-associated calcium transients (Milojkovic et al. 2007).

Modeling the results of the channel blocker experiments suggest that the sodium and calcium channel currents make a relatively minor contribution to the total charge flowing, around 10–20% (Schiller et al. 2000); to a first approximation, this is consistent with the calcium profiles, taking into account indicator saturation in the high calcium zone and the fact that the total current through NMDAR channels is about 10-fold higher than their calcium flux (Garaschuk et al. 1996).

Bigger glutamate pulses lead to longer duration plateaus and more extensive high calcium zones, with progressively stronger saturation of fluorescence close to the input site. Saturation is more severe if higher affinity indicators are used, blurring the distinction between the input site high calcium zone and the distal zone (see Methods; compare with Cai et al. 2004; Milojkovic et al. 2007; Wei et al. 2001).

How small an active NMDAR conductance zone can generate an NMDA spike?

The high calcium zones are only around 10–25 μm in extent just above spike/plateau threshold (Fig. 5). Significant axial calcium diffusion along a dendrite is likely to be restricted to ~10 μm or less, judging from the spatial extent of calcium transients proximal to the input site which continue to rise after the end of a spike/plateau (e.g., Figure 4*A*, blue traces). Alternatively, we can define an 'approximate diffusion distance' to be the radius at half-amplitude of the Gaussian-shaped solution to the diffusion equation, at a given time t, in response to an impulse of calcium. This distance is $\sim 1.67(Dt)^{1/2}$, where D is the calcium diffusion coefficient (see Supplementary Information). Assuming a D of 100 $\mu m^2/s$ (Loewenstein and Sompolinsky 2003) - at the high end of the likely range - gives an approximate calcium diffusion distance of ~3.3 μm after 40 ms, the typical duration of just supra-threshold NMDA spikes (Fig. 5). The approximate diffusion distance doubles to ~6.7 μm when the diffusion time is quadrupled to 160 ms (about the duration of the plateaus in Fig. 4*A* and *B*), a reasonable match to the actual spatial extent of the calcium transients exhibiting a delayed rise. The low affinity Magnesium Green calcium indicator we used does not pick up calcium transients associated with single action potentials, but it saturates with long-duration NMDA plateaus. The indicator's dynamic range is well-matched to the calcium transients from short-duration NMDA spikes; it is also sensitive enough, generally, to detect the distal zone lower amplitude calcium transients from all but very brief NMDA spikes. The pattern of calcium influx seen with this indicator can therefore serve as a semi-quantitative rough guide to the spatial profile of the active NMDAR conductance zone dominating the electrogenesis of a spike/plateau. If anything, the active NMDAR zone will fall slightly within the high calcium zone due to smearing by calcium diffusion.

From the above we can say that a) each dendrite contains several times as much NMDAR conductance as the minimum required for an NMDA spike, b) as a focal glutamate stimulus grows, so the active NMDAR conductance zone grows, c) when the glutamate input site is moved, the active NMDAR conductance zone moves with it, and d) the minimum size of active NMDAR conductance zone required to support an NMDA spike grows about 2.5-fold from distal to proximal, from around 10 μm to 25 μm in half-width. This is qualitatively consistent with the fivefold growth in glutamate thresholds, and the sevenfold growth in local input conductance, maximal sub-threshold responses at the soma and NMDA spike somatic amplitudes. The discrepancy between the growth in the active zone size and the other measures suggests the possibility that, in our experiments, at threshold a higher density of NMDAR conductances may be activated within more proximal active zones.

What is a 'computational subunit'? Potential versus functional subunits

As mentioned, we define a decision-making computational subunit to be a device which emits a clear signal above some defined threshold level of graded input. Here we mean a part of a dendrite receiving a wide dynamic range of inputs which can initiate a spike or plateau potential. We define a '*potential*' computational subunit to be a stretch or segment of dendrite which has the *capability* of firing an NMDA spike. More restrictively, we define a '*functional*' computational subunit to be a dendritic segment whose *actual* local *I-V* curve is *at least bistable at least part of the time* (Supplementary Fig. S4). In other words, the segment should at least temporarily contain enough active (bound) NMDAR conductance so that a sufficiently large transient local depolarization could flip it into an UP-state. 'At least bistable' includes cases where the *I-V* curve is in the 'mono-stable UP' regime (Supplementary Fig. S4), in which case the segment spontaneously fires an NMDA spike/plateau. For two *functional* subunits to co-exist in a single dendrite, they should exhibit distinguishable input-output relations: the *location* of the inputs should make a difference to the output.

Co-operativity between functional subunits

Depolarizing drive from nearby active zones could make the local *I-V* curve in a segment of dendrite bistable at lower levels of active NMDAR conductance. In our experiments, NMDA spike threshold exhibited an approximately linear trade-off between glutamate and baseline voltage (Fig. 6). This might provide a biophysical basis for different dendritic regions to

interact co-operatively: depolarization from one could reduce the glutamate thresholds of others. Distal plateaus could help trigger proximal ones in the same dendrite, as well as prolonging their duration (extrapolating from Fig. 5*C*). Compartmental model simulations demonstrating these potential interactions are shown in Supplementary Figs. S5 and S6. Similarly, in other simulations (not shown), plateau generation in different dendrites interacts co-operatively across branch points, or even across the cell body, depending on the propagation of depolarizations (Nevian et al. 2007). The average somatic membrane potential during action potential firing driven by NMDA plateaus is depolarized relative to baseline (e.g., Figure 7), and this depolarization propagates into neighboring dendrites (Milojkovic et al. 2004, 2005a,b, 2007). Simulations also suggest that local inhibition should be able to reduce these interactions (Rhodes 2006; G. Major, unpublished results).

How many computational subunits is a basal dendrite equivalent to?

Our experiments show that, beyond about 10–20 μm of the branch point, all segments of a terminal basal dendrite longer than ~10 μm (distally) to ~25 μm (proximally) can generate an NMDA spike. (Within 10–20 μm of the branch point our stimuli could not generally be localized to a single dendrite). Terminal basal dendrites are typically 100–200 μm long (Larkman 1991a; Larkman et al. 1992). Around five to ten NMDA spike high calcium zones, and hence suprathreshold active NMDAR conductance zones, could fit into this length - possibly more. Therefore a single basal dendrite in a brain slice could function as a continuum or string of multiple *potential* subunits. The somatic amplitude of the spike/plateau would encode the location of the subunit generating it.

Models using biologically plausible parameters demonstrate that, in principle, multiple *functional* subunits could also coexist in a single basal dendrite, if they were sufficiently separated in space and/or time. For example, three tonically-activated, *spatially*-separated bistable NMDAR conductance zones can be fitted within a single simulated basal dendrite (Supplementary Fig. S5), such that an UP-state in a more distal zone does not trigger an UP-state in a more proximal active zone. This dendrite behaves as three distinct functional subunits, capable of generating three very different amplitude NMDA spikes, depending on which of the bistable active zones receives a coincident burst of brief excitatory inputs big enough to depolarize it across threshold. More simultaneously active functional subunits could in principle be fitted into a single dendrite, separating them using higher membrane conductance or cytoplasmic resistivity, or bands of inhibitory conductance, all of which can impede forward propagation of NMDA spikes (simulations not shown). Longer dendrites could also accommodate more functional subunits.

In simulations, NMDA spike propagation can also be impeded by reducing the *temporal* overlap between activation of different NMDAR zones. If two identical inputs are given sequentially to a proximal and then to a distal compartment, separated by a few tens of milliseconds, and then the stimuli are reversed, very different responses can result. If the distal input is large enough to trigger an NMDA spike by itself, but the proximal input is not, then proximal followed by distal can lead to a small somatic response, whereas if the distal input arrives first, the resulting depolarization can help the proximal compartment cross NMDA spike threshold, yielding a much bigger somatic response (Supplementary Fig. S6). Such co-operativity between multiple cascaded dynamic subunits could potentially allow single terminal dendrites to perform very sophisticated computations. For example, again in simulations, a sweep of excitatory inputs from distal to proximal can be tuned so that a 'chain reaction' of NMDA spikes propagates from one subunit to the next, resulting in a large somatic response, whereas in the opposite direction, proximal NMDA spike initiation fails, giving a small somatic response: directional selectivity at the level of a single dendrite (G.M., unpublished).

On the other hand, simulations also suggest that a single terminal dendrite may behave as a *single* functional subunit under some conditions, as suggested in previous studies (Losonczy and Magee 2006; Wei et al. 2001). In particular, a brief, spatially distributed pulse of glutamatergic input spread uniformly along a single basal dendrite can produce a plateau potential with a peak somatic amplitude that is graded with stimulus strength, accompanied by a characteristic slowly-declining plateau-top (Supplementary Fig. S7). This is terminated by a rapid switch-off once NMDAR deactivation leads to a loss of bistability in the most terminal part of the dendrite (Supplementary Fig. S4). If the AMPAR/NMDAR ratio is low enough, as might occur during repetitive activity (Armstrong-James et al. 1993; Augustinaite and Heggelund 2007; Chen et al. 2002; Wu et al. 2004), there is still a distinct jump in amplitude at a particular threshold stimulus level, but the amplitude continues to increase thereafter, in contrast to the saturation seen with focal stimuli. These simulations show that *distributed* inputs, which may be more likely in vivo than focal stimuli, could in principle generate NMDA spike/plateaus. Interestingly, similar declining plateau-tops were observed at high stimulus levels in brain slice experiments, perhaps in part because of an extended zone of activated NMDARs (e.g., Supplementary Fig. S7, bottom right).

The abstraction of a single basal dendrite as a cascade of multiple co-operating dynamic subunits (Fig. 8) is helpful for intuitively understanding its computational potential. We predict that the *functional* subunits of a sufficiently long thin dendrite could depend on its actual *anatomical and temporal input pattern*.

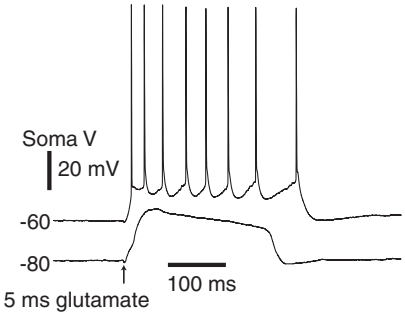

FIG. 7. Dendritic NMDA spike/plateaus can support persistent firing. A brief (5 ms) pulse of glutamate onto a basal dendrite (in this case, 83 μm from soma) can elicit persistent firing outlasting the stimulus by hundreds of milliseconds. Hyperpolarization reveals the underlying plateau potential.

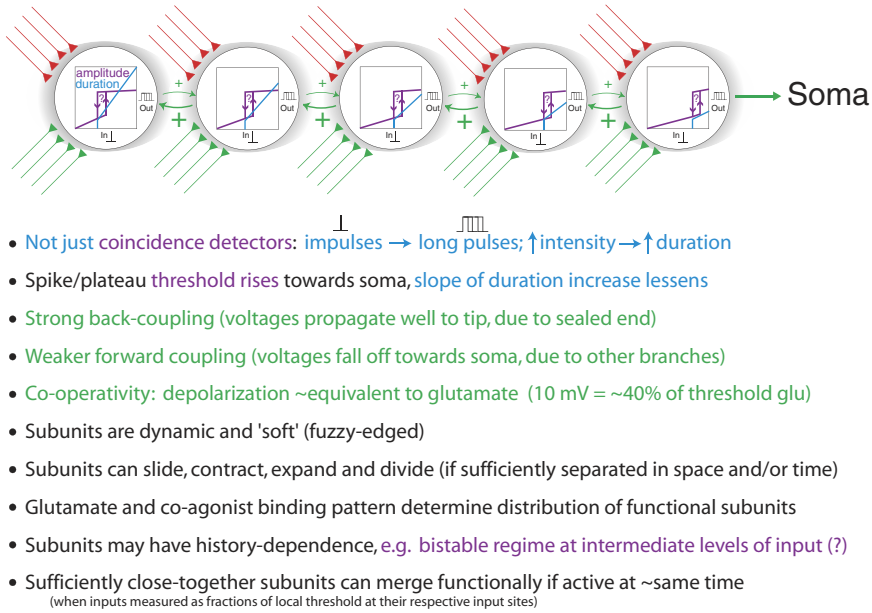

FIG. 8. Schematic of working hypothesis that a single basal dendrite can be equivalent to a cascade of multiple co-operating "soft-edged" dynamic subunits. Inputs: excitatory (green) and inhibitory (red). Each subunit has 2 outputs: *voltage* (purple) and, above threshold, the *duration* of the spike/plateau (blue). Durations of distal plateaus increase more steeply with glutamate than those of proximal plateaus (data not shown). The somatic amplitude falls with input distance from the soma because of the weak forward coupling between subunits, which is also in large part responsible for their predicted cooperativity: the glutamate-depolarization trade-off for NMDA spike threshold is indicated by the notional equivalence between glutamate and voltage inputs into a given subunit. Depending on conditions, a subunit may have a bistable regime, indicated by the hysteretic loops in the input-output-amplitude relations (purple): brief positive or negative inputs of sufficient amplitude can flip the state of a bistable subunit (Supplementary Fig. S4). The "soft edge" and dynamic nature of each subunit is indicated by gray shading; in cases of smooth input distributions, boundaries between subunits will be somewhat arbitrary. Close-together subunits may merge functionally (see Supplementary Information).

A role for NMDA plateaus in graded persistent firing?

In vitro, a single basal dendrite can perform far more than a simple instantaneous thresholding operation. Spike/plateaus evoked by focal stimulation are graded both spatially *and* temporally, duration increasing with both glutamate and depolarization (Fig. 5). In addition to their possible role in coincidence detection, NMDAR-dominated spike/plateaus could therefore contribute to temporal integration within and across dendrites, and to sequence generation. In response to strong but brief stimuli, basal dendrites can produce plateau potentials lasting hundreds of milliseconds (Fig. 5*B*), resulting in persistent firing of a similar duration if action potential threshold is crossed (Fig. 7). Even a distal spike/plateau might have an appreciable effect on action potential output if a cell is close to threshold or is already firing. The strong spatial gradient in plateau amplitudes makes this mechanism naturally suited for supporting graded persistent neural firing (Funahashi et al. 1991; Romo et al. 1999), which is thought to contribute to working memory (Lisman et al. 1998; Major and Tank 2004). Consistent with this, both persistent firing and working memory are disrupted by NMDAR antagonists (Aultman and Moghaddam 2001; Aura and Riekkinen 1999; Castner and Williams 2007; Dudkin et al. 2001), which can also cause psychosis (Coyle et al. 2003).

In our experiments it is possible that plateau potentials may have been prolonged by slow clearance of extracellular glutamate. However, our models suggest that long duration plateaus can result from brief impulses of glutamate, by virtue of the slow de-activation kinetics of the NMDA receptor (see Methods and Supplementary Fig. S7). Nevertheless, whatever the time course of the glutamate transient, the presence or absence of a plateau potential may signal potentially important information for its duration. For example, models suggest that a slow glutamate transient resulting in sufficient (but not too many) bound NMDARs might make a stretch of dendrite bistable for a period of time (Supplementary Fig. 4). If there was no subsequent suprathreshold depolarizing input, the dendrite would stay in the DOWN-state. However, a brief, sufficiently large depolarizing input could flip the dendrite into an UP-state lasting until the bistability ended (Supplementary Fig. 5), or until a sufficiently large hyperpolarizing input flipped it back into the DOWN-state.

Low micromolar background or tonic levels of glutamate may occur in vivo (Cavelier et al. 2005), as well as prolonged glutamate transients due to repetitive firing. Both may favor NMDA spike/plateaus by desensitizing AMPA receptors and by priming NMDARs (Patneau and Mayer 1990; Trussell and Fischbach 1989). Indeed, the ratio of NMDAR to AMPAR currents is not fixed, but increases during repetitive trains of synaptic stimuli (Armstrong-James et al. 1993; Augustinaite and Heggelund 2007; Chen et al. 2002; Wu et al. 2004).

Prevalence of local dendritic spike/plateaus

Several labs have between them found local dendritic spike/plateaus in terminal dendrites in slices from several neocortical areas and from hippocampus. They can be evoked using three different techniques: glutamate uncaging, iontophoresis and synaptic stimulation. They occur in all three major classes of terminal dendrite in pyramidal neurons - basals, apical obliques and apical tufts (Ariav et al. 2003; Holthoff et al. 2004; Milojkovic et al. 2004; Schiller et al. 2000; Wei et al. 2001; Major and Schiller, unpublished data). There is still some debate about the ionic mechanisms underlying these events,

which may reflect genuine variations between different dendrite classes, cell types and brain areas. In particular, there seems to be a greater contribution from sodium currents in hippocampal pyramidal cell basal and oblique dendrites (Ariav et al. 2003; Losonczy and Magee 2006).

Why should we care about NMDA spikes? It is worth pointing out that NMDARs have evolved to have strong electrogenic effects far beyond simply letting calcium into neurons: only about $\sim 10 \pm 5\%$ of the charge flowing through them is actually calcium (Garaschuk et al. 1996; Jahr and Stevens 1993; Schneggenburger 1996; Schneggenburger et al. 1993). NMDARs have a huge influence on moment-to-moment information processing and neural firing in the brain, on top of their more generally acknowledged role in plasticity (Daw et al. 1993; Rivadulla et al. 2001). NMDA plateau potentials are known to play a key role in spinal chord circuits during rhythmic locomotion (Grillner 2003; Schmidt et al. 1998), and it is plausible that similar machinery may be used by other brain areas. NMDA spikes can produce LTP (Gordon et al. 2006), and hence in principle they could contribute to the self-organization of clustered inputs, and increase the probability of their own occurrence. In any case, simulations show *distributed* inputs to a single branch can generate NMDA spike/plateaus (Supplementary Fig. 7), and in the case of distal NMDA spikes, only a dozen or so synapses may need to be activated over a relatively long 10–20 ms time window (Rhodes 2006). NMDA spikes are therefore compatible with the much-debated possibility of sparse neural firing during behavior (Brecht 2007; Shoham et al. 2006; Yao et al. 2007). Sparse occurrence of NMDA spikes may have the added benefit of reducing the associated dendritic calcium burden but may also make these events harder to find in vivo.

The robustness and prevalence of terminal dendritic spike/plateaus in vitro suggest that it is worth looking for them in vivo. An exhaustive search for NMDA spike/plateaus in cerebral cortex in behaving animals has yet to be undertaken, and is likely to be technically challenging. Our results suggest that low affinity calcium indicators or reporter proteins should be used to distinguish between the large calcium transients associated with NMDA spikes and the smaller calcium transients associated with back-propagating action potentials and synaptic activity.

Conclusion

We have shown that brief focal glutamate pulses onto neocortical pyramidal neuron terminal basal dendrites can elicit dendritic NMDAR conductance-dominated spike/plateau potentials with:

a) somatic amplitudes that are strongly graded with input location,

b) thresholds that exhibit a linear trade-off between glutamate and depolarization, and

c) durations that increase both with glutamate and depolarization.

With focal inputs, NMDA spike/plateaus are generated mainly by an 'active' NMDAR conductance zone, the glutamate-bound conductance declining with distance from the center of the input. The minimum (threshold) active zone ranges in half-width from ~ 25 μm for proximal input locations down to ~ 10 μm for distal locations, increasing in size with the amplitude of the glutamate input and the spike/plateau duration. Neocortical basal dendrites therefore appear to be endowed with ample biophysical machinery for supporting highly versatile computational capabilities, although it is still not known to what extent NMDA spike/plateaus occur during behavior in vivo. Because the input-output relations of neocortical basal dendrites can be dominated by NMDAR conductances, network activity patterns may dynamically reconfigure what these dendrites can actually compute. At times, a particular terminal dendrite may simply gather and filter inputs, functioning as part of a larger computational unit, such as the neuron. At other times a single terminal dendrite may function as a computational subunit in its own right. Depolarization reduces glutamate thresholds, providing a biophysical basis for potential interactions between different dendritic regions. Simulations exploring this demonstrate that if appropriately timed and physically localized activated regions of a dendrite exist in vivo, then a single terminal dendrite could correspond to a cascade of *multiple* co-operating dynamic decision-making subunits, each capable of retaining information for hundreds of milliseconds, with influence on neural output increasing from distal to proximal. In some senses, this latter scenario may represent an upper bound on the capabilities of a single dendrite, based on the biophysical machinery we have demonstrated in brain slices. What actually occurs in behaving animals remains to be seen.

ACKNOWLEDGMENTS

We thank J. A. Miri for help with early stages of the data analysis, M. Hines for help with NEURON, and B. Mel for useful discussions.

Present address of G. Major: School of Biosciences, Cardiff University, UK.

GRANTS

Cardiff University, the Royal Society, the Wellcome Trust, and the BBSRC supported G. Major during later stages of this work.

REFERENCES

Ariav G, Polsky A, Schiller J. Submillisecond precision of the input-output transformation function mediated by fast sodium dendritic spikes in basal dendrites of CA1 pyramidal neurons. *J Neurosci* 23: 7750–7758, 2003.

Armstrong-James M, Welker E, Callahan CA. The contribution of NMDA and non-NMDA receptors to fast and slow transmission of sensory information in the rat SI barrel cortex. *J Neurosci* 13: 2149–2160, 1993.

Ascher P, Nowak L. The role of divalent cations in the *N*-methyl-D-aspartate responses of mouse central neurones in culture. *J Physiol* 399: 247–266, 1988.

Augustinaite S, Heggelund P. Changes in firing pattern of lateral geniculate neurons caused by membrane potential dependent modulation of retinal input through NMDA receptors. *J Physiol* 582: 297–315, 2007.

Aultman JM, Moghaddam B. Distinct contributions of glutamate and dopamine receptors to temporal aspects of rodent working memory using a clinically relevant task. *Psychopharmacology* 153: 353–364, 2001.

Aura J, Riekkinen P Jr. Blockade of NMDA receptors located at the dorsomedial prefrontal cortex impairs spatial working memory in rats. *Neuroreport* 10: 243–248, 1999.

Brecht M. Barrel cortex and whisker-mediated behaviors. *Curr Opin Neurobiol* 17: 408–416, 2007.

Brodin L, Traven HG, Lansner A, Wallen P, Ekeberg O, Grillner S. Computer simulations of *N*-methyl-D-aspartate receptor-induced membrane properties in a neuron model. *J Neurophysiol* 66: 473–484, 1991.

Cai X, Liang CW, Muralidharan S, Kao JP, Tang CM, Thompson SM. Unique roles of SK and Kv4.2 potassium channels in dendritic integration. *Neuron* 44: 351–364, 2004.

Carnevale NT, Hines ML. *The Neuron Book.* Cambridge, UK: Cambridge Univ. Press, 2006.

Cash S, Yuste R. Linear summation of excitatory inputs by CA1 pyramidal neurons. *Neuron* 22: 383–394, 1999.

Castner SA, Williams GV. Tuning the engine of cognition: A focus on NMDA/D1 receptor interactions in prefrontal cortex. *Brain Cogn* 63: 159–187, 2007.

Cavelier P, Hamann M, Rossi D, Mobbs P, Attwell D. Tonic excitation and inhibition of neurons: ambient transmitter sources and computational consequences. *Prog Biophys Mol Biol* 87: 3–16, 2005.

Chen C, Blitz DM, Regehr WG. Contributions of receptor desensitization and saturation to plasticity at the retinogeniculate synapse. *Neuron* 33: 779–788, 2002.

Coyle JT, Tsai G, Goff D. Converging evidence of NMDA receptor hypofunction in the pathophysiology of schizophrenia. *Ann NY Acad Sci* 1003: 318–327, 2003.

D'Angelo E, Rossi P, Taglietti V. Voltage-dependent kinetics of *N*-methyl-D-aspartate synaptic currents in rat cerebellar granule cells. *Eur J Neurosci* 6: 640–645, 1994.

Davis GW. Homeostatic control of neural activity: from phenomenology to molecular design. *Annu Rev Neurosci* 29: 307–323, 2006.

Daw NW, Stein PS, Fox K. The role of NMDA receptors in information processing. *Annu Rev Neurosci* 16: 207–222, 1993.

Dudkin KN, Kruchinin VK, Chueva IV. Neurophysiological correlates of delayed visual differentiation tasks in monkeys: the effects of the site of intracortical blockade of NMDA receptors. *Neurosci Behav Physiol* 31: 207–218, 2001.

Euler T, Detwiler PB, Denk W. Directionally selective calcium signals in dendrites of starburst amacrine cells. *Nature* 418: 845–852, 2002.

Funahashi S, Bruce CJ, Goldman-Rakic PS. Neuronal activity related to saccadic eye movements in the monkey's dorsolateral prefrontal cortex. *J Neurophysiol* 65: 1464–1483, 1991.

Garaschuk O, Schneggenburger R, Schirra C, Tempia F, Konnerth A. Fractional Ca^{2+} currents through somatic and dendritic glutamate receptor channels of rat hippocampal CA1 pyramidal neurones. *J Physiol* 491: 757–772, 1996.

Gordon U, Polsky A, Schiller J. Plasticity compartments in basal dendrites of neocortical pyramidal neurons. *J Neurosci* 26: 12717–12726, 2006.

Grillner S. The motor infrastructure: from ion channels to neuronal networks. *Nat Rev Neurosci* 4: 573–586, 2003.

Haugland RP, Free KE. Fluorescent Ca^{2+} indicators. In: *Molecular Probes Handbook.* Eugene, OR: Invitrogen, 2005a p. 19.13.

Haugland RP, Free KE. Fluorescent Mg^{2+} indicators. In: *Molecular Probes Handbook.* Eugene, OR: Invitrogen, 2005b p. 19.16.

Haugland RP, Free KE. http://probes.invitrogen.com/handbook/figures/0703.html, Figure 19.5. In: *Molecular Probes Handbook* (10th ed.). Eugene, OR: Invitrogen, 2006, chapt. 19, p. 19.75.

Holthoff K, Kovalchuk Y, Yuste R, Konnerth A. Single-shock LTD by local dendritic spikes in pyramidal neurons of mouse visual cortex. *J Physiol* 560: 27–36, 2004.

Jahr CE, Stevens CF. Calcium permeability of the *N*-methyl-D-aspartate receptor channel in hippocampal neurons in culture. *Proc Natl Acad Sci USA* 90: 11573–11577, 1993.

Koester HJ, Sakmann B. Calcium dynamics associated with action potentials in single nerve terminals of pyramidal cells in layer 2/3 of the young rat neocortex. *J Physiol* 529: 625–646, 2000.

Larkman AU. Dendritic morphology of pyramidal neurones of the visual cortex of the rat. I. Branching patterns. *J Comp Neurol* 306: 307–319, 1991a.

Larkman AU. Dendritic morphology of pyramidal neurones of the visual cortex of the rat. III. Spine distributions. *J Comp Neurol* 306: 332–343, 1991b.

Larkman AU, Major G, Stratford KJ, Jack JJ. Dendritic morphology of pyramidal neurones of the visual cortex of the rat. IV. Electrical geometry. *J Comp Neurol* 323: 137–152, 1992.

Lisman JE, Fellous J-M, Wang X-J. A role for NMDA-receptor channels in working memory. *Nat Neurosci* 1: 273–275, 1998.

Loewenstein Y, Sompolinsky H. Temporal integration by calcium dynamics in a model neuron. *Nat Neurosci* 6: 961–967, 2003.

Losonczy A, Magee JC. Integrative Properties of Radial Oblique Dendrites in Hippocampal CA1 Pyramidal Neurons. *Neuron* 50: 291–307, 2006.

Major G, Larkman AU, Jonas P, Sakmann B, Jack JJ. Detailed passive cable models of whole-cell recorded CA3 pyramidal neurons in rat hippocampal slices. *J Neurosci* 14: 4613–4638, 1994.

Major G, Tank D. Persistent neural activity: prevalence and mechanisms. *Curr Opin Neurobiol* 14: 675–684, 2004.

Mason A, Larkman A. Correlations between morphology and electrophysiology of pyramidal neurons in slices of rat visual cortex. II. Electrophysiology. *J Neurosci* 10: 1415–1428, 1990.

Matsuzaki M, Ellis-Davies GC, Nemoto T, Miyashita Y, Iino M, Kasai H. Dendritic spine geometry is critical for AMPA receptor expression in hippocampal CA1 pyramidal neurons. *Nat Neurosci* 4: 1086–1092, 2001.

Milojkovic BA, Radojicic MS, Antic SD. A strict correlation between dendritic and somatic plateau depolarizations in the rat prefrontal cortex pyramidal neurons. *J Neurosci* 25: 3940–3951, 2005a.

Milojkovic BA, Radojicic MS, Goldman-Rakic Tl TP, Antic SD. Burst generation in rat pyramidal neurones by regenerative potentials elicited in a restricted part of the basilar dendritic tree. *J Physiol* 558: 193–211, 2004.

Milojkovic BA, Wuskell JP, Loew LM, Antic SD. Initiation of sodium spikelets in basal dendrites of neocortical pyramidal neurons. *J Membr Biol* 208: 155–169, 2005b.

Milojkovic BA, Zhou WL, Antic SD. Voltage and calcium transients in basal dendrites of the rat prefrontal cortex. *J Physiol* 585: 447–468, 2007.

Nakayama S, Nomura H, Tomita T. Intracellular-free magnesium in the smooth muscle of guinea pig taenia caeci: a concomitant analysis for magnesium and pH upon sodium removal. *J Gen Physiol* 103: 833–851, 1994.

Nevian T, Larkum ME, Polsky A, Schiller J. Properties of basal dendrites of layer 5 pyramidal neurons: a direct patch-clamp recording study. *Nat Neurosci* 10: 1–9, 2007.

Oakley JC, Schwindt PC, Crill WE. Dendritic calcium spikes in layer 5 pyramidal neurons amplify and limit transmission of ligand-gated dendritic current to soma. *J Neurophysiol* 86: 514–527, 2001a.

Oakley JC, Schwindt PC, Crill WE. Initiation and propagation of regenerative Ca(2+)-dependent potentials in dendrites of layer 5 pyramidal neurons. *J Neurophysiol* 86: 503–513, 2001b.

Patneau DK, Mayer ML. Structure-activity relationships for amino acid transmitter candidates acting at *N*-methyl-D-aspartate and quisqualate receptors. *J Neurosci* 10: 2385–2399, 1990.

Poirazi P, Brannon T, Mel BW. Pyramidal neuron as two-layer neural network. *Neuron* 37: 989–999, 2003.

Pologruto TA, Sabatini BL, Svoboda K. ScanImage: flexible software for operating laser scanning microscopes. *Biomed Eng Online* 2: 13, 2003.

Polsky A, Mel BW, Schiller J. Computational subunits in thin dendrites of pyramidal cells. *Nat Neurosci* 7: 621–627, 2004.

Rall W. Core conductor theory and cable properties of neurons. In: *Handbook of Physiology. The Nervous System. Cellular Biology of Neurons,* edited by Kandel ER. Bethesda, MD: Am. Physiol. Soc., 1977, sect. 1, vol. I, part 1, p. 39–98.

Rhodes P. The properties and implications of NMDA spikes in neocortical pyramidal cells. *J Neurosci* 26: 6704–6715, 2006.

Rivadulla C, Sharma J, Sur M. Specific roles of NMDA and AMPA receptors in direction-selective and spatial phase-selective responses in visual cortex. *J Neurosci* 21: 1710–1719, 2001.

Romo R, Brody CD, Hernandez A, Lemus L. Neuronal correlates of parametric working memory in the prefrontal cortex. *Nature* 399: 470–473, 1999.

Schiller J, Major G, Koester HJ, Schiller Y. NMDA spikes in basal dendrites of cortical pyramidal neurons. *Nature* 404: 285–289, 2000.

Schiller J, Schiller Y. NMDA receptor-mediated dendritic spikes and coincident signal amplification. *Curr Opin Neurobiol* 11: 343–348, 2001.

Schmidt BJ, Hochman S, MacLean JN. NMDA receptor-mediated oscillatory properties: potential role in rhythm generation in the mammalian spinal cord. *Ann NY Acad Sci* 860: 189–202, 1998.

Schneggenburger R. Simultaneous measurement of Ca^{2+} influx and reversal potentials in recombinant *N*-methyl-D-aspartate receptor channels. *Biophys J* 70: 2165–2174, 1996.

Schneggenburger R, Zhou Z, Konnerth A, Neher E. Fractional contribution of calcium to the cation current through glutamate receptor channels. *Neuron* 11: 133–143, 1993.

Seamans JK, Yang CR. The principal features and mechanisms of dopamine modulation in the prefrontal cortex. *Prog Neurobiol* 74: 1–58, 2004.

Shoham S, O'Connor DH, Segev R. How silent is the brain: is there a "dark matter" problem in neuroscience? *J Comp Physiol A Neuroethol Sens Neural Behav Physiol* 192: 777–784, 2006.

Stratford K, Mason A, Larkman AU, Major G, Jack JJ. The modelling of pyramidal neurons in the visual cortex. In: *The Computing Neuron*, edited by Durbin R, Miall C, Mitchison G. Wokingham, UK: Addison-Wesley, 1989, p. 296–321.

Trevelyan AJ, Jack J. Detailed passive cable models of layer 2/3 pyramidal cells in rat visual cortex at different temperatures. *J Physiol* 539: 623–636, 2002.

Trussell LO, Fischbach GD. Glutamate receptor desensitization and its role in synaptic transmission. *Neuron* 3: 209–218, 1989.

Wang D, Grillner S, Wallen P. Effects of flufenamic acid on fictive locomotion, plateau potentials, calcium channels and NMDA receptors in the lamprey spinal cord. *Neuropharmacology* 51: 1038–1046, 2006.

Wei DS, Mei YA, Bagal A, Kao JP, Thompson SM, Tang CM. Compartmentalized and binary behavior of terminal dendrites in hippocampal pyramidal neurons. *Science* 293: 2272–2275, 2001.

Wolosker H. NMDA receptor regulation by D-serine: new findings and perspectives. *Mol Neurobiol* 36: 152–164, 2007.

Wu SH, Ma CL, Kelly JB. Contribution of AMPA, NMDA, and GABA(A) receptors to temporal pattern of postsynaptic responses in the inferior colliculus of the rat. *J Neurosci* 24: 4625–4634, 2004.

Yao H, Shi L, Han F, Gao H, Dan Y. Rapid learning in cortical coding of visual scenes. *Nat Neurosci* 10: 772–778, 2007.

Zhao M, Hollingworth S, Baylor SM. Properties of tri- and tetracarboxylate Ca^{2+} indicators in frog skeletal muscle fibers. *Biophys J* 70: 896–916, 1996.